Temporal variability of repolarization in rat ventricular myocytes paced with time-varying frequencies

Massimiliano Zaniboni, Francesca Cacciani and Nicolò Salvarani

(Experimental Physiology **92:859-869, 2007***)*

State of the art

Action potential generation by a single cardiac cell

For a single cardiac cell under space-clamp conditions, the following equation relates the transmembrane potential (V_m) to the total transmembrane ionic current (I_{ion})

$$(1) \quad dV_m/dt = -1/C_m * I_{ion}$$

where C_m is the membrane capacitance (1 μF/cm^2) provided by the charge separation across the lipid bilayer (Fozzard, 1966). Equation (1) simply states that changes in V_m occur due to displacement of charge on the membrane capacitance by the movement of ions across the cell membrane. This movement occurs via voltage-gated ion channels, pumps, and exchangers, I_{ion} in Figure 1. A negative I_{ion} (inward flow of positive ions into the cell) produces a positive dV_m/dt, which elevates (depolarizes) the membrane potential. A positive I_{ion} indicates an outward flow of positive ions and acts to reduce (repolarize) the membrane potential by generating a negative dV_m/dt. Importantly, in a single, space-clamped cell (Weidmann, 1955), generation of the AP results from the time, voltage, and concentration-dependent evolution of I_{ion}, which represents the contribution of many ion-selective mechanisms for ion movement across the membrane. Figure 2 is a schematic diagram of a cardiac ventricular cell and its electrophysiological components. It also serves to illustrate a mathematical model of the mammalian cardiac ventricular cell [the Luo-Rudy (LRd) model] that computes the AP from membrane currents carried by ionic channels, pumps, and exchangers. This model accounts for dynamic changes

in ionic concentrations during the AP (including Na^+, K^+, and Ca^{2+}) and their effects on the membrane ionic currents and provides the basis for the quantitative description of AP generation. The AP and selected ionic currents that generate the AP and determine its morphology and duration are shown in figure 3. Once activation threshold is reached, the fast inward sodium current (I_{Na}) depolarizes the membrane at a very fast rate and generates the fast AP upstroke. I_{Na} reaches a very large peak magnitude and quickly inactivates (Figure 3b). When the V_m upstroke reaches about -25 mV, the inward L-type calcium current [$I_{Ca(L)}$] (Figure 3c) activates and provides a depolarizing current that supports the AP plateau against the repolarizing action of the outward delayed potassium currents I_{Kr} (r = rapid) and I_{Ks} (s = slow) (Figure 3e). It plays an important role in triggering Ca^{2+} release from the sarcoplasmic reticulum (SR) through the calcium-induced calcium release (CICR) mechanism (Fabiato et al., 1985) to generate the calcium transient and initiate contraction. The dome of $I_{Ca(L)}$ maintains the plateau; it slowly declines as L-type calcium channels inactivate. The two repolarizing potassium currents, I_{Kr} and I_{Ks}, gradually increase during the plateau, shifting the balance of currents in the outward direction to repolarize the membrane towards its resting potential. The sodium/calcium exchanger (I_{NaCa}) is an electrogenic process with a 3 Na^+: 1 Ca^{2+} stochiometry (Eisner et al., 1985) (Figure 3d). Early during the AP it operates in its "reverse mode" to extrude Na^+ from the cell, generating a small outward current (Crespo et al., 1990). It then reverses direction and operates in its "direct mode" to extrude Ca^{2+}, becoming a significant inward current that acts to slow repolarization during the late plateau and prolongs the AP duration (Earn et al., 1990).

Finally, there is a large increase (late peak) of the outward (inward rectifier) potassium current I_{K1}, that dominates the late repolarization phase and the return of the membrane to its resting level (Figure 3g). The Luo-Rudy model does not include the transient outward current I_{to}. This current is not expressed in guinea pig ventricle or in endocardial cells of other species but it is present in rat ventricle. In its presence, a "notch" is created in the AP following its peak upstroke, a process termed "phase 1 repolarization" (Figure 3f). According to Figure 3, it is clear that two ionic currents, I_{Na} and $I_{Ca(L)}$, are the major contributors of depolarizing charge during the AP. In many cardiac arrhythmias, such as in ventricular and atrial fibrillation, the head of a propagating wave interacts with the phase of repolarization of a preceding wave. Under such circumstances membrane ion channels affecting AP

repolarization may become important determinants of impulse conduction, in addition to I_{Na} and $I_{Ca(L)}$.

Main currents in the Ventricular action potential of rat

The main inward currents flowing in the rat ventricular action potential are:

(1) the fast inward sodium current (I_{Na}); the activation of I_{Na} is at about –60 mV and is very fast, the inactivation occurs in 1-2 ms; the inactivation is then removed in 1-10 ms when the membrane potential returns to the resting value; it is blocked by tetrodoxin (TTX) (Fozzard & Hanck, 1996) (Figure 3b);

(2) the inward L-type calcium current [$I_{Ca(L)}$]; the activation of $I_{Ca(L)}$ is at about –40 mV and is more slow than I_{Na} (the activation time is about of 8 ms). The inactivation is either voltage- or calcium dependent (Lee et al, 1985). It is blocked by nifedipine (Figure 3c).

The main outward currents are:

(3) the transient outward current (I_{to}); the activation of I_{to} is at about –20 mV during the depolarization and is pretty fast. The inactivation is removed during the diastolic period with a time constant that is, in ventricular myocytes, about 20 ms (Apkon & Nerbonne, 1991). It is blocked by 4-aminopyridine (4-AP) (Figure 3f). In the left ventricle its density is maximum at the epicardium and is minor in the other layers of the ventricular wall (Clark et al, 1993);

(4) the outward delayed potassium currents I_{Kr} (r = rapid) and I_{Ks} (s = slow). (Sanguinetti et al,1990) (Figure 3e);

(5) the outward inward rectifier potassium current I_{K1}; it is the main current during the late repolarization phase (Tourner et al, 1987) (Figure 3g).

Spatial dispersion of the rat ventricular repolarization

Myocardium APs show a remarkable heterogeneity, for example between atrial and ventricular cells, between ventricles apex and base and between the different layers of the left ventricular wall (Figure 4).

Apex/base differences in rat action potential duration (APD) have been demonstrated by Watanabe et al. (1983). They found that endocardial action potentials recorded

from ventricular wall preparations could be classified by duration into short (found in basal, mid, and apical regions of the right ventricle), intermediate (in mid and apical regions of the left ventricle), and long (basal left ventricle). They also found that myocytes isolated from the whole of both ventricles showed a range of APD that could be divided into three groups and appeared to correspond to the three types recorded from tissue preparations. However, they did not explore possible endocardial/epicardial differences in APD or attempt to isolate myocytes from specific regions. Shipsey et al. (1997) demonstrated that APD of subendocardial myocytes is longer than those of subepicardial myocytes in normal rat hearts (Figure 5). They found that regional differences in action potential amplitude (APA) and APD_{25} are still detectable in the presence of 4-AP, which suggests that although I_{to} density may be greater in subepicardial than in subendocardial myocytes the magnitude of other rapidly activating currents must also differ between regions. They also compared the electrophysiology of midmyocardial cells to subepicardial and subendocardial myocytes in the rat. The action potential parameters of midmyocardial cells are intermediate between the values for subendocardial and subepicardial cells at all stimulation frequencies studied (0.2, 1.0, and 2.0 Hz).

Effect of the pacing rate on the APD

An important principle can be drawn regarding the ionic basis of the various phases of the AP. In a normal ventricular myocyte, the rising phase (AP upstroke) is a robust "all or none" process that is dominated by a single large ionic current, I_{Na}. In contrast, the plateau and repolarization phases are determined by a delicate balance between several smaller inward and outward currents. This distinction is consistent with physiologic function. Robustness and large factor of safety are required properties of the rising phase, insuring dependable AP generation and excitation. The plateau and repolarization phases, however, require flexibility and adaptability under tight control. These properties are important for the adaptation of the AP to physiologic changes in heart rate. With an increase in heart rate, APD shortens to adapt to the new, shorter cycle length of excitation (a process termed APD rate-dependency). The dependence of APD on several opposing process (inward and outward currents), and the delicate balance between them, provides high sensitivity (small changes in individual currents can cause large APD changes) and multiplicity

of "control points" for optimal control. In the guinea pig model simulation (LRd ventricular cell model) APD decreases by close to 50 % from its steady state value when the pacing cycle length is reduced from 1000 to 200 msec (not shown). The mechanism of APD shortening with increasing rate involves several ionic currents. Most importantly, I_{Ks} is augmented at the fast rate because of incomplete deactivation (residual activation) of this slowly deactivating current during the short diastolic interval between APs. Also, plateau I_{NaCa} is enlarged in the outward direction ("reverse") because of $[Na^+]_i$ accumulation at the fast rate, contributing to the adaptation process. It should be recognized that the ionic mechanisms of APD adaptation are species dependent. For example, in the canine, the relative rate of deactivation of I_{Ks} and I_{Kr} is reversed from that in the guinea pig. In the guinea pig, I_{Ks} is slow to deactivate, a property that makes this current sensitive to rate changes and a major participant in APD adaptation. In the canine, I_{Ks} deactivates much faster (faster than I_{Kr}) ; therefore, it cannot contribute as much to APD adaptation, suggesting a more prominent role for I_{Kr} and possibly $I_{Ca(L)}$ in this process.

Rat ventricular myocytes show a rate-dependent prolongation of APD secondary to a decrease in the transient outward current (I_{to}) (Shigematsu et al, 1997, figure 6), which is prominent in rat and is the main determinant of the early repolarization phase (Josephson et al., 1984). Recovery of I_{to} from inactivation is incomplete at the higher frequencies and so it is strongly depressed as the rate of stimulation is increased. This rate-dependent prolongation is significantly inhibited in the presence of 4-aminopyridine (4-AP) (figure 7), a blocker of the transient outward K^+ current (I_{to}). Human action potentials also show a reduced early repolarization phase as frequency increases, which is also thought to be due to partial inactivation of I_{to}. Wettwer et al. (1993) directly compared I_{to} in rat and human isolated myocytes and found that the kinetics of inactivation are similar, especially when the faster physiological heart rate of rats is taken into account. For what regard the late repolarization phase, the myocytes of the three layers of the ventricular wall show different behaviors in presence of an increasing stimulation frequency. Briefly, switching from low to high pacing rate, the subepicardial APs tend to prolong, midmyocardial APs substantially don't change while subendocardial APs show rate-dependent shortening. The mechanism of this shortening is due to three factors: 1) incomplete removal of the inward L-type calcium current $I_{Ca(L)}$ inactivation; 2) hyperactivity of the electrogenic sodium/potassium pump (I_{NaK}): during

depolarization a big amount of sodium enters in the cell through the membrane channels. More frequently the cell is stimulated, more sodium enters in the cell, and more the sodium/potassium pump (I_{NaK}) has to be activated to reestablish the proper Na^+ gradient. This process tends to repolarize the membrane because its $3Na^+$ out : $2K^+$ stochiometry; 3) the electrogenic sodium/calcium exchanger (I_{NaCa}) during the rat ventricular myocyte diastole has a reversal potential more negative than the resting membrane potential, and so the exchanger tends to store up calcium in the cytoplasm (Maier et al, 2000) instead of removing it from the cell (the electrogenic sodium/calcium exchanger in the heart rat works in "reverse" mode rather than in "direct mode", repolarizing the membrane). In conditions of high pacing rate, the time interval for storing calcium inside the cell diminishes and the low concentration of Ca^{2+} inside the cell determines an activity reduction of the sodium/calcium exchanger, with consequent shortening of the action potential.

Electrical restitution

Electrical restitution of a cell paced with a train of pulses at a constant pacing rate followed by a pre/post-mature stimulus is the relationship between APD of the pre/post-mature beat and the preceding CL or DI. This is a general property of cardiac tissues (Figure 9), and is clinically important because in ischemic conditions ventricular arrhythmias are frequently initiated following a premature beat and experiments to investigate the electrical restitution curve may provide important clues to arrhythmogenesis and its control. In particular, electrical restitution is considered a potential target for anti-arrhythmic therapies (Gilmour et al., 2003) following the discovery that flattening the restitution curve can prevent the transition from tachycardia to ventricular fibrillation (VF; Garfinkel et al., 2000).

In multicellular mammalian preparations (Bass et al., 1975), as well as in single cardiomyocytes (Robinson et al., 1987), the restitution process is believed to be governed by the time-dependent changes of those ion currents which control cardiac action potential. According to the diversity in types, density and kinetics of the ion channels in various cardiac membranes, significant interspecies differences in the restitution kinetics have been reported (Carmeliet 1977). There are, however, relatively few data published on the electrical restitution in rat ventricular muscle (Poggesi et al., 1987). Nanasi et al. (1996) studied the mechanism of electrical

restitution in isolated rat ventricular muscle using drugs that inhibit specific ion currents. Their preparations were continuously paced using a train of 20 basic stimuli delivered at a cycle length of 1000 ms. These trains of basic stimuli were interrupted by a single extra stimulus applied at successively longer coupling intervals. In this way, each 20th basic action potential was followed by a single extra action potential occurring at successively longer diastolic intervals. The diastolic interval (DI) was defined as a time elapsed from the APD_{90} of the last basic action potential of the train to the upstroke of the extra action potential. They generated restitution curves by plotting the duration of each extra action potential (APD_{50}) against its DI. This restitution relation, mesasured in Tyrode solution at 37° C, was best described as a sum of three exponential components. When DI was gradually increased from its initial value of 10 ms, action potential duration rapidly increased until reaching its longest value around DI = 50 ms. After this peak, action potential duration decreased first rapidly, then slowly, as DI was further increased up to 4s (figure 10). Therefore they blocked the specific ion channels that control repolarization of the action potential in order to evaluate their contribution to the restitution process. Inhibition of I_{to} by 4-AP significantly increased APD_{50}. Inhibition of $I_{Ca(L)}$ by nifedipine significantly decreased APD_{50}. Regarding the kinetics of restitution, 4-AP did not alter the time constant of any of the three components resolved, however, the relative amplitudes of these components (except for the third component) were significantly increased by 4-AP. Inhibition of $I_{Ca(L)}$ by nifedipine fully abolished the original first and second components, while the third component was relatively unaffected. The restitution relation observed in the presence of nifedipine decayed monotonically with biexoponential kinetics. The time constant of the first, very rapid negative component was ranging between 5 and 20 ms, while that of the late negative component ranged between 500 and 1000 ms. These results indicate that the normal peformance of restitution requires functionally intact Ca^{2+} channels (figure 11 and 12). In addition, “dynamic restitution”, defined as the relationship between each APD and the preceding DI during VF, has been studied (Watanabe et al., 2002). Nevertheless, an account of the dynamic restitution properties of single ventricular myocytes and its interplay with intrinsic temporal dispersion of APD is still lacking in physiological pacing conditions.

Beat-to-beat variability of APD_{90} in isolated myocytes

Rhythm and duration of beats vary and they are subjected to 1) extrinsic (e.g., baroreflex, autonomic nervous system control etc.) and 2) intrinsic control (e.g., rate-dependency, restitution, duration of refractory period etc.). An abnormal increase in rhythm variability is one of the mechanisms involved in arrhythmogenesis. In fact irregularities of the heartbeat due to cardiac electric dysfunction are one of the most frequent causes of mortality and morbidity in the human population, especially in cases of cardiac failure as an end-stage syndrome of a variety of Cardiac diseases (Myerburg et al., 1997). Variability may be also found at cellular level and in the beating rate of the pacemaker cells (Wilders & Jongsma, 1993), or in the duration of the ventricular action potentials (Zaniboni et al, 2000, figure 13). In particular, the temporal variability of cellular action potentials duration, when it is not suppressed by the electrotonic interactions with neighboring cells, is considered a possible source of arrhythmic events classically described as “triggered activity”. In the most dangerous cases, it may even lead to a ventricular fibrillation or to a sudden cardiac death. Zaniboni et al. (2000) showed that single guinea pig ventricular myocytes paced at a constant rate and held at a constant temperature exhibit beat-to-beat variations in APD. It was found that repolarization variability is a random process and that the CV (SD/mean APD_{90}) was relatively independent of APD, yielding a mean of 2.3%. Figure 13 C shows a histogram of APD_{90} from 200 consecutive action potentials recorded in a guinea pig myocyte. APD_{90} was normally distributed around a mean value of 342.8 ms with an SD of 10.4 ms. A correlation coefficient of 0.92 between a Gaussian fit and the histogram indicated that APD_{90} variability within a cell was a random process. It seems likely that beat-to-beat variability in APD results from stochastic behavior of ion channels activated during plateau and repolarization. In fact the partial block of currents involved in the repolarization by means of pharmacological agents (e.g., TTX, EGTA) has been shown to modulate this variability.

Several important studies have established a close association between temporal dispersion of ventricular repolarization and vulnerability to arrhythmias (Laurita et al., 1998). It is clear from the earlier discussion that disease-induced changes in ion channel expression in the heart can produce dispersions of repolarization that play a central role in the pathophysiology of functionally determined reentrant circuits.

Relation between the cardiac electric activity recorded on the body surface (ECG) and in the single cells (action potential)

As the heart undergoes depolarization and repolarization, the electrical currents that are generated spread not only within the heart, but also throughout the body. Fluctuations in potential can be recorded extracellularly. This electrical activity generated by the heart can be measured by electrodes placed on the body surface. The recorded tracing is called an electrocardiogram (ECG; figure 14). The P wave is produced by atrial depolarization, the QRS complex by ventricular depolarization, and the ST segment and T wave by ventricular repolarization. After inscription of the P wave, the ECG returns to its baseline because changing potential differences within the heart are no longer recorded at the body surface. The interval between the P wave and the QRS complex represents an important index of impulse propagation through the AV node, AV bundle, and bundle branches. The time needed for the impulse to pass from the atria to the ventricles can be estimated from the P-R interval which extends from the beginning of the P wave to the first deflection of the QRS complex. The QRS complex records potentials at the body surface generated when the wave of depolarization passes through the ventricular myocardium. The amplitude of the QRS complex is greater than that of the P wave because the ventricular mass is greater than that of the atria. Following the inscription of the QRS complex, the ECG returns to its baseline where it remains until the inscription of the T wave. This isoelectric phase, S-T segment, occurs when all regions of the ventricle are in a depolarized state, during the plateau (phase 2) of the ventricular action potential. The duration of the S-T segment thus reflects the normally long plateau of the cardiac action potential. In the rat the S-T segment is not isoelectric, presumably because of the high current density of I_{to} which accelerates the process of repolarization: in this way a gradient of potential is always present (Gussak et al,2000). Repolarization of the ventricles generates the T wave, which corresponds to the end of phase 2 and phase 3 of the cardiac action potential. The duration of the T wave is considerably longer than that of the QRS complex because, unlike ventricular depolarization, repolarization does not spread as a rapidly propagated wave. The Q-T interval provides a useful index of the ventricular action potential duration. Measurements of the Q-T interval, along with determinations of the duration of the QRS complex,

allow clinical evaluation of the effect of drugs and diseases on the electrical activity of the heart (Surawicz and Knoebel, 1984). The Q-T duration is frequently measured as a function of R-R interval, which is the inverse of the cardiac frequency (Figure 15). Both R-R and Q-T interval have their counterparts respectively in firing rate of nodal cells and APD of ventricular cardiomyocytes. Both this cellular parameters display an intrinsic variability (Wilders & Jongsma, 1993; Zaniboni et al., 2000) which can in principle contribute to the variability recorded at the ECG level. Beat-to beat Q-T R-R relationship can be viewed as a measure of beat-to-beat (dynamic) electrical restitution (Lux et al., 1998). In healthy subjects, this relationship has been shown to be characterized by high inter-subject variability and high intra-subject stability (Batcharov et al. 2002). Abonormalities in sinus rhythm variability, cellular repolarization variability and their relationship could be mechanisms of still unclarified cardiac pathologies, like sudden cardiac death. The main electrical mechanisms of this disease are ventricular tachycardia, ventricular fibrillation and asystole.

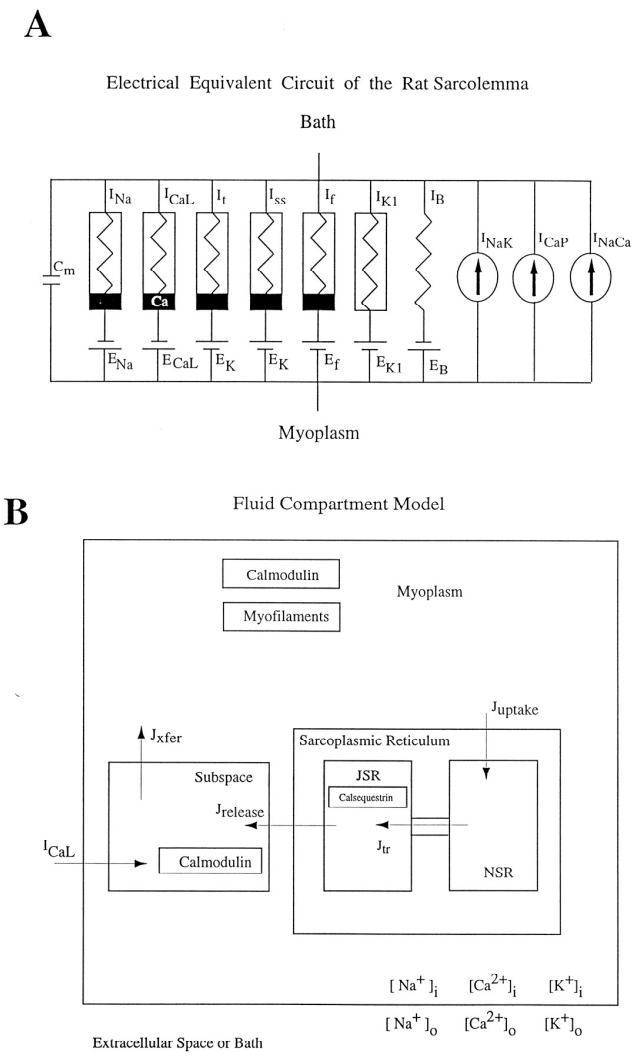

Figure 1. Electrical equivalent circuit. *(A) Electrical equivalent circuit of the adult rat epicardial/endocardial ventricular cell. (B) Fluid compartment model of the rat cardiac cell (epi and endocardial). The expressions for the intracellular Ca^{2+} dynamics are based on the work of Winslow et al., 1999.*

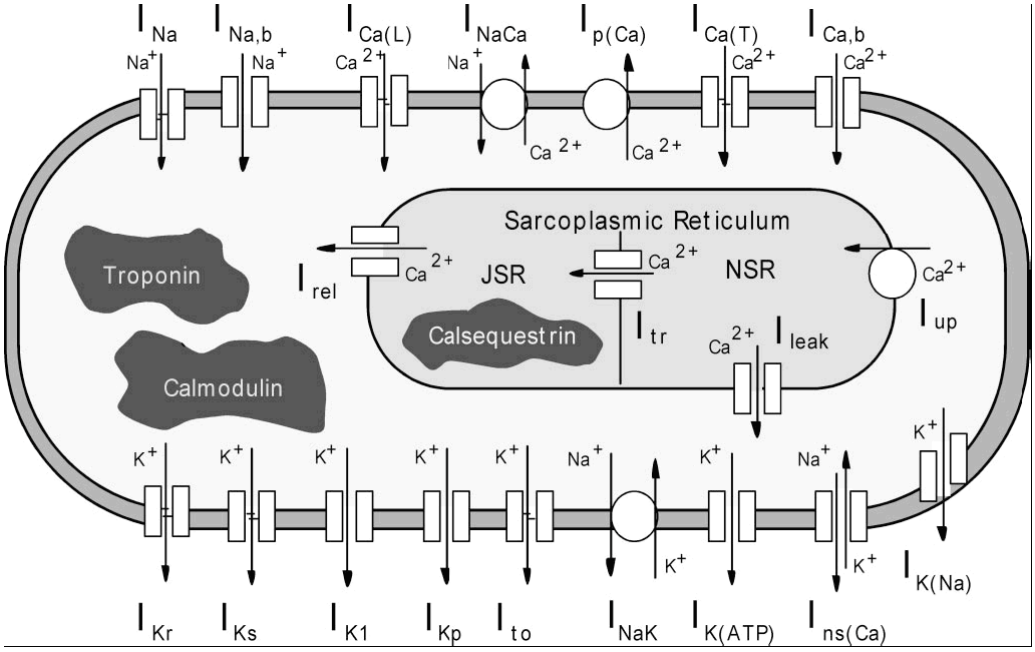

Figure 2. Ion currents of the ventricular AP. *Schematic diagram of the dynamic Luo-Rudy (LRd) ventricular cell model. I_{Na}, fast sodium current; $I_{Ca(L)}$, calcium current through L-type calcium channels; $I_{Ca(T)}$, calcium current through T-type calcium channels; I_{kr}, rapid delayed rectifier potassium current; I_{ks}, slow delayed rectifier potassium current; I_{to}, transient outward current; I_{K1}, inward rectifier potassium current; $I_{K(ATP)}$, ATP-sensitive potassium current; I_{Kp}, plateau potassium current; $I_{K(Na)}$, sodium-activated potassium current (activated under conditions of sodium overload); $I_{ns(Ca)}$, nonspecific calciumactivated current (activated under conditions of calcium overload); $I_{Na,b}$, sodium background current; $I_{Ca,b}$, calcium background current; I_{NaK}, sodium-potassium pump current; I_{NaCa}, sodium-calcium exchange current; $I_{P(Ca)}$, sarcolemnal calcium pump; I_{up}, calcium uptake from the myoplasm to the network sarcoplasmic reticulum (NSR); I_{rel}, calcium release from junctional sarcoplasmic reticulum (JSR); I_{leak}, calcium leakage from NSR to the myoplasm; I_{tr}, calcium translocation from NSR to JSR. Calmodulin and troponin are calcium buffers in the myoplasm. Calsequestrin is a calcium buffer in the JSR.*

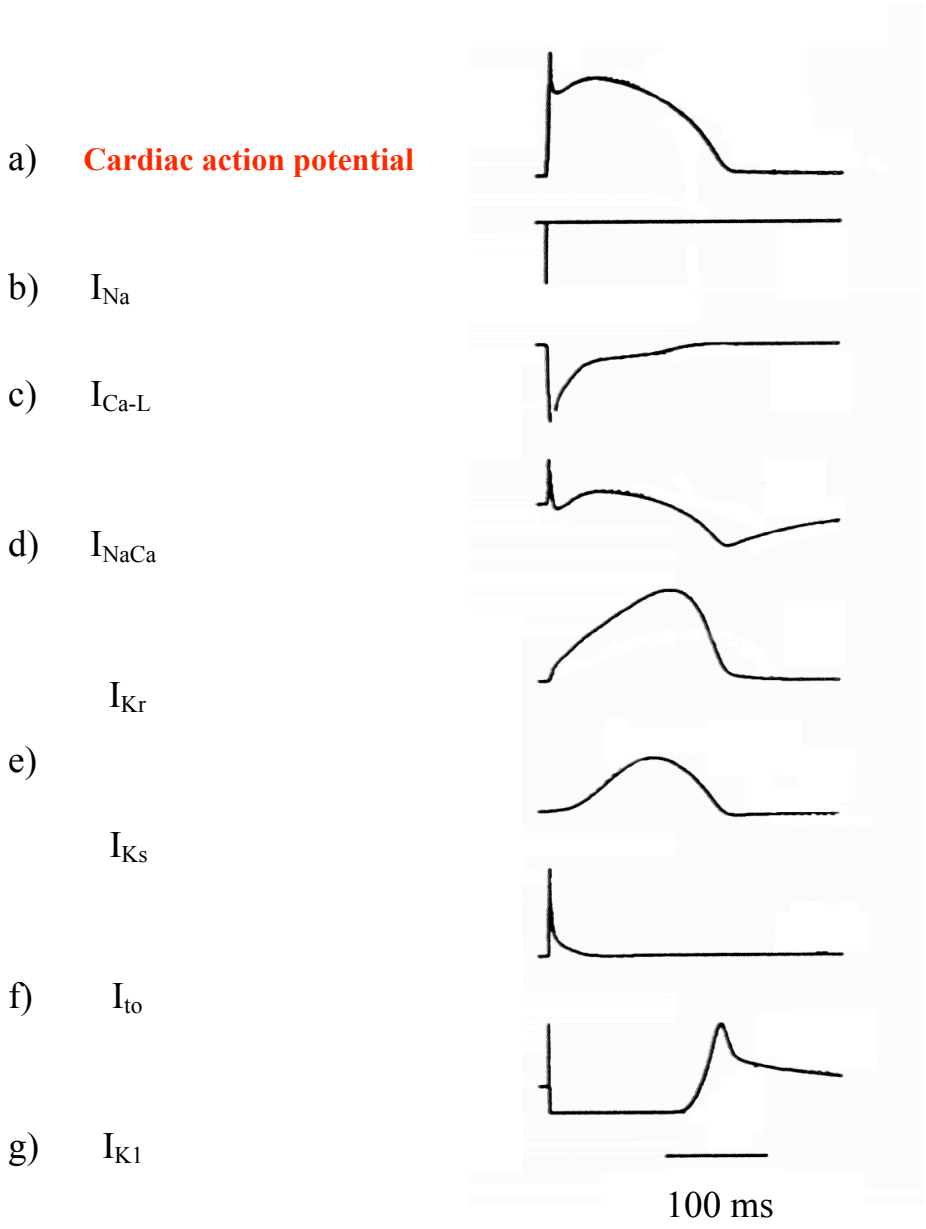

Figure 3. Major ionic currents during the AP. *Shown are the AP (a), and selected ionic currents that determine the AP morphology b), c), d), e), f) and g) (Currents symbol are defined in figure 1).*

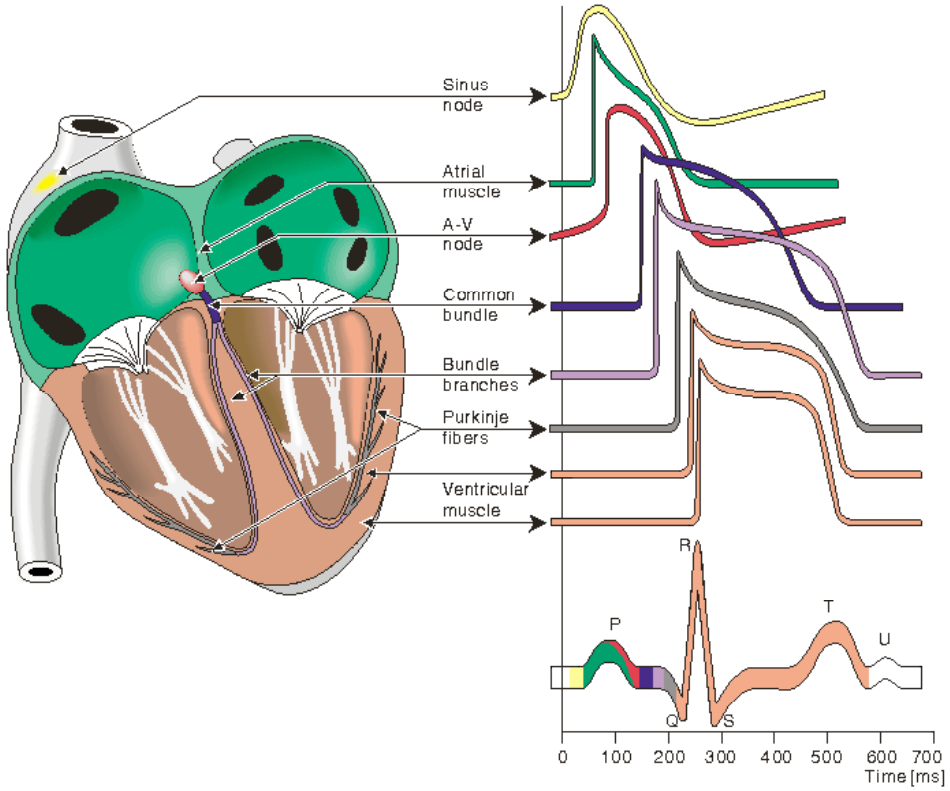

Figure 4. Electrophysiology of the heart. *The different waveforms for each of the specialized cells found in the heart are shown. The latency shown approximates that normally found in the healthy heart.*

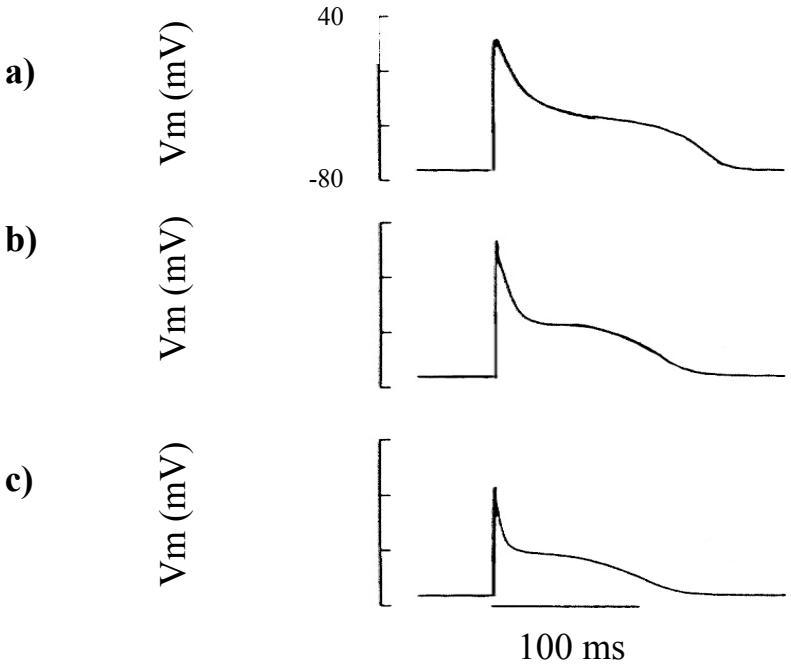

Figure 5. Spatial dispersion of ventricular repolarization. *Representative single action potentials recorded from subendocardial (a) to, midmyocardial (b), and subepicardial (c) myocytes isolated from rat left ventricle. (From Shipsey et al, 1997).*

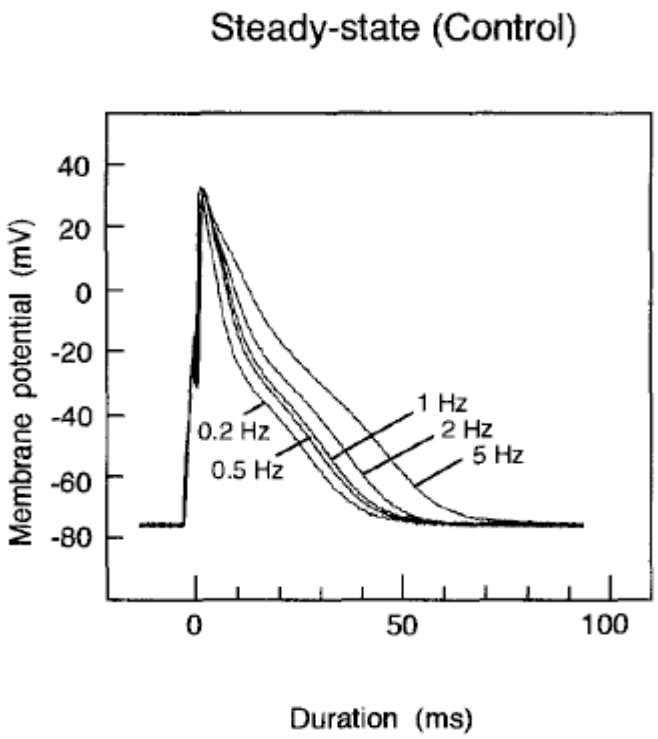

Figure 6. Rate-dependency of APD. *Superimposed traces indicate the steady-state action potentials, stimulated at 0.2, 0.5, 1, 2, and 5 Hz, as indicated. The duration of action potentials is prolonged as the stimulation frequency is increased. (From Shigematsu et al, 1997).*

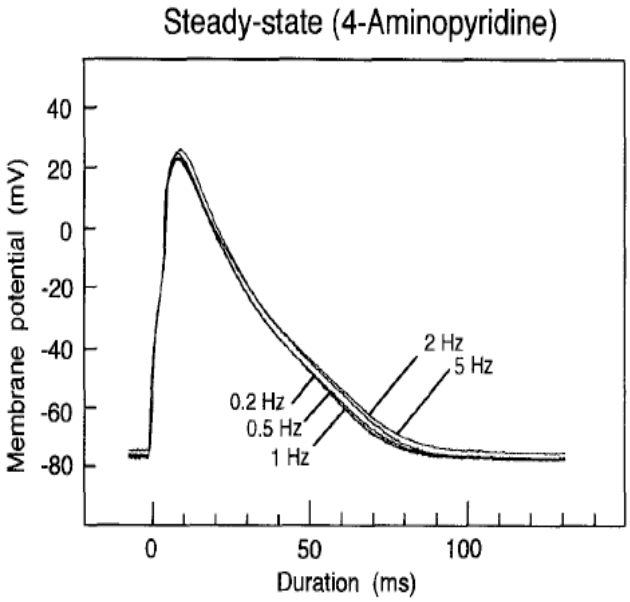

Figure 7. Rate-dependency of APD. *Superimposed traces indicate the steady-state action potentials, stimulated at 0.2, 0.5, 1, 2, and 5 Hz, as indicated. Note that the application of 4-AP significantly lengthened the action potential duration (APD) at all stimulation frequencies and abolished the rate-dependent prolongation of APD. (From Shigematsu et al, 1997).*

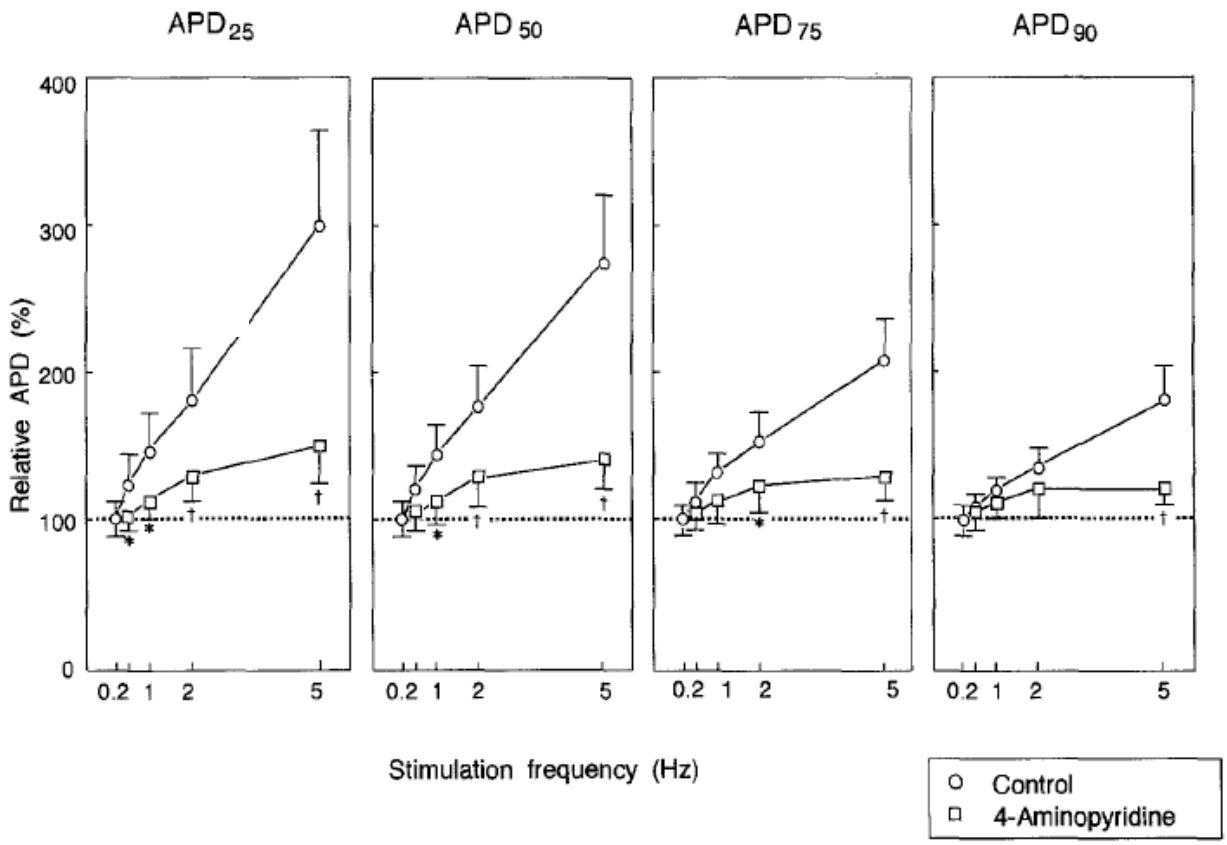

Figure 8. Relationship between the stimulation frequency and APD. *The APDs are compared at 25 % (APD_{25}), 300 50 % (APD_{50}), 75 % (APD_{75}), and 90 % (APD_{90}) levels of repolarization. APDs are presented as percent of the APD at 0.2 Hz for each repolarization level (Relative APD). In the presence of 4-AP, the rate dependent APD prolongation was significantly inhibited at all 100 levels tested. Values are presented as means ± SEM. *p < 0.05, †< 0.01; significant difference from the APD in control condition (without 4- AP) at respective stimulation frequency, n = 6 in control, n = 4 in the presence of 4-AR. (From Shigematsu et al, 1997).*

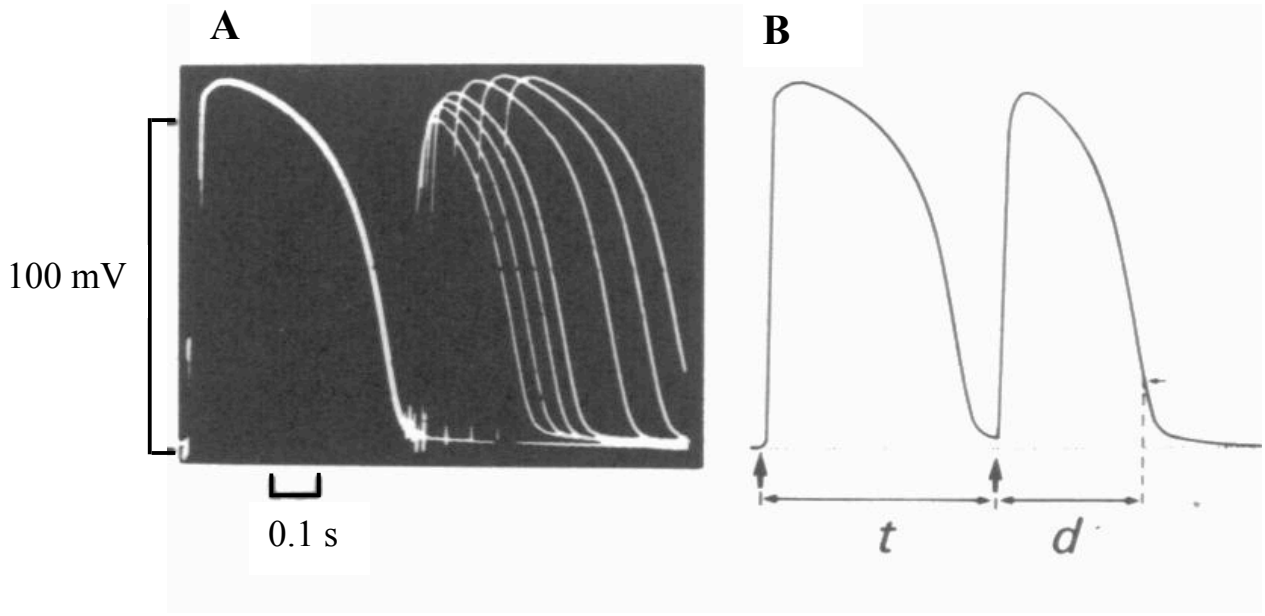

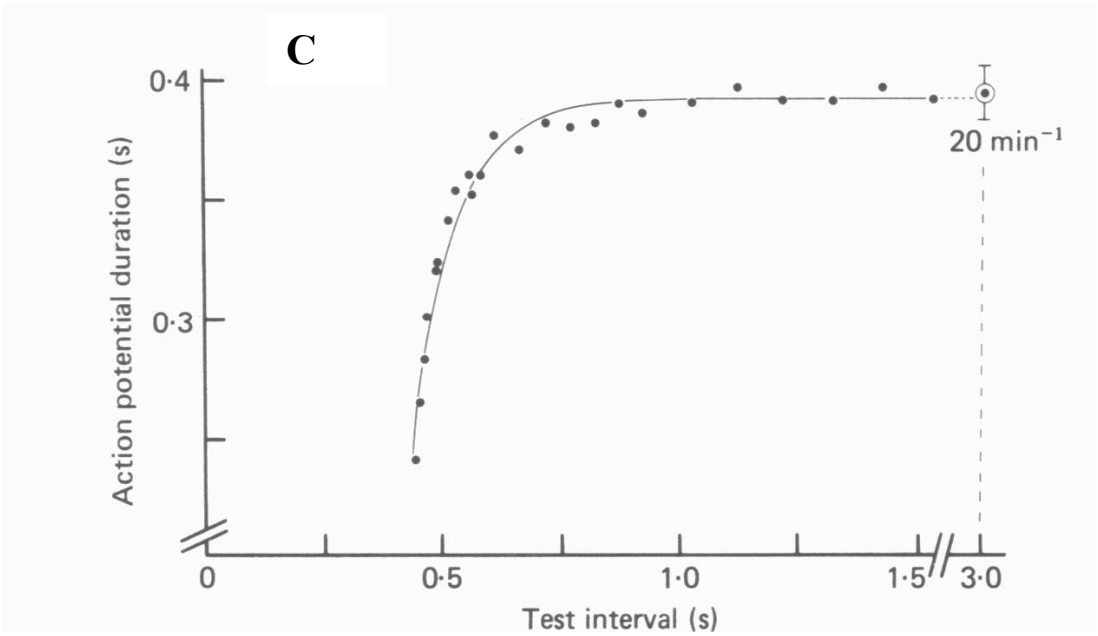

Figure 9. Electrical restitution curve. *A) Superimposed oscilloscope records of regular (control) action potentials followed by test responses at various stimulus intervals. B) Schematic diagram to illustrate the measurement of test interval between stimuli (t) and action potential duration at 80% repolarization (d). C) Graph showing how the duration of the test action potential (d in panel B) varied with the test interval (t in panel B). The circled point shows the mean duration of regular action potentials at 20 min^{-1} with bars giving ±1I S.D. (n = 30). (From Boyett & Jewell, 1978)*

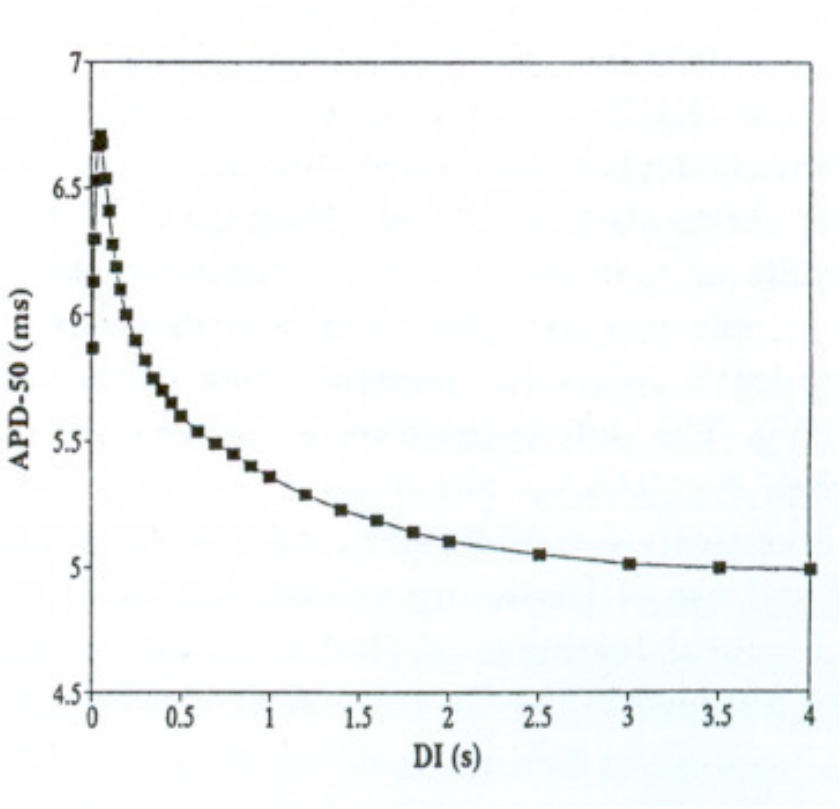

Figure 10. Electrical restitution curve established in rat ventricular muscle. *a) Electrical restitution relation established by plotting the APD_{50} value of each extra action potential against the respective diastolic interval (n = 9). Basic cycle length of 1000 ms. (From Nanasi et al., 1996).*

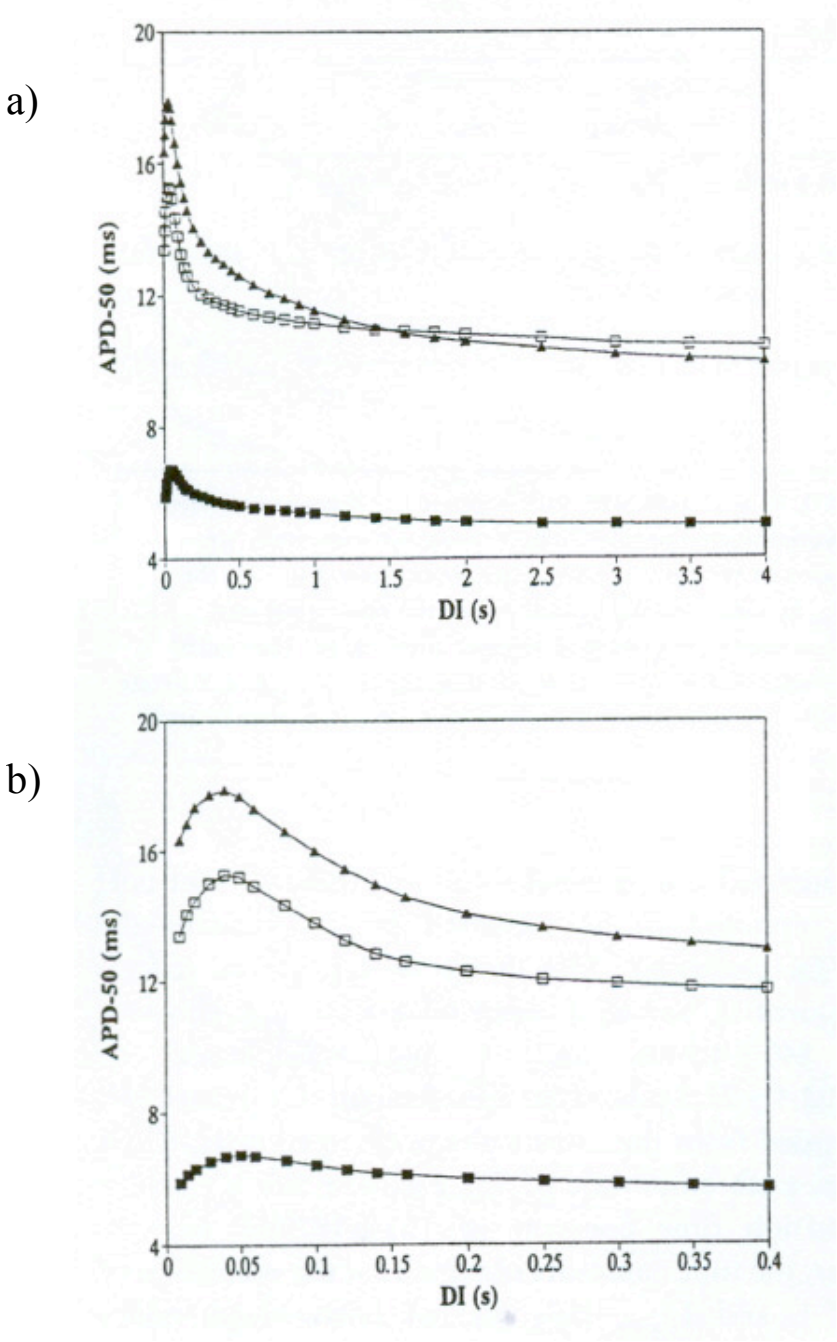

Figure 11. Electrical restitution curves obtained in Tyrode and in the presence of 4-AP and TEA. *A) Electrical restitution relations obtained in Tyrode solution (filled squares, n = 9) in presence of 4-AP (open squares, n = 9) and in Tea-loaded preparations (triangles, n = 4). The initial exponential part of (a) (for DI between 0 and 400 ms) is shown in (b) on exponential time scale. (From Nanasi et al., 1996).*

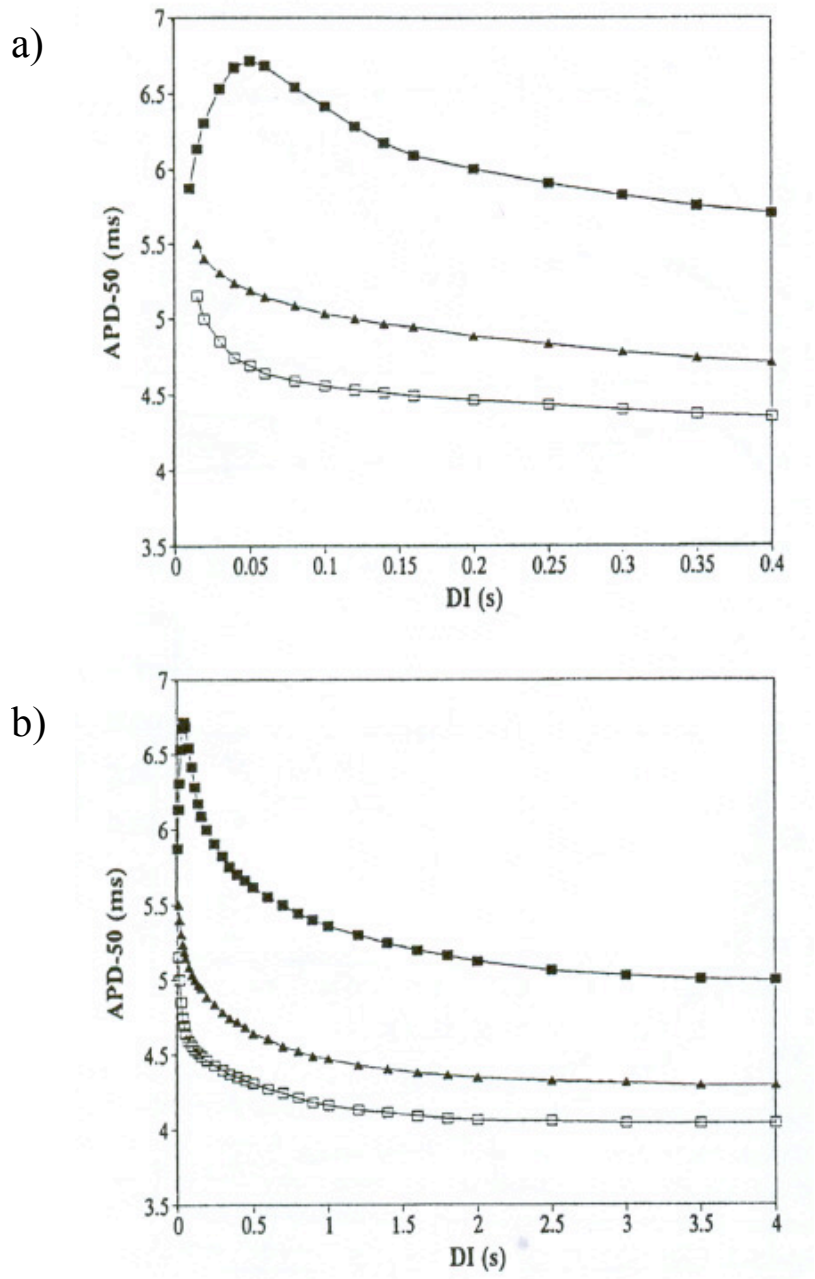

Figure 12. Electrical restitution curves obtained in Tyrode and in the presence of nifedipine and $MnCl_2$. *a) Effect of nifedipine (open squares, n = 8) and $MnCl_2$ (triangles, n = 10) on the restitution relation. Filled squares represent the control record obtained in Tyrode solution (n = 9) at BCL = 100 ms. In (a), the initial 400 ms of the curve, while in (b), the full range of DIs applied (up to 4s) is depicted. (From Nanasi et al., 1996).*

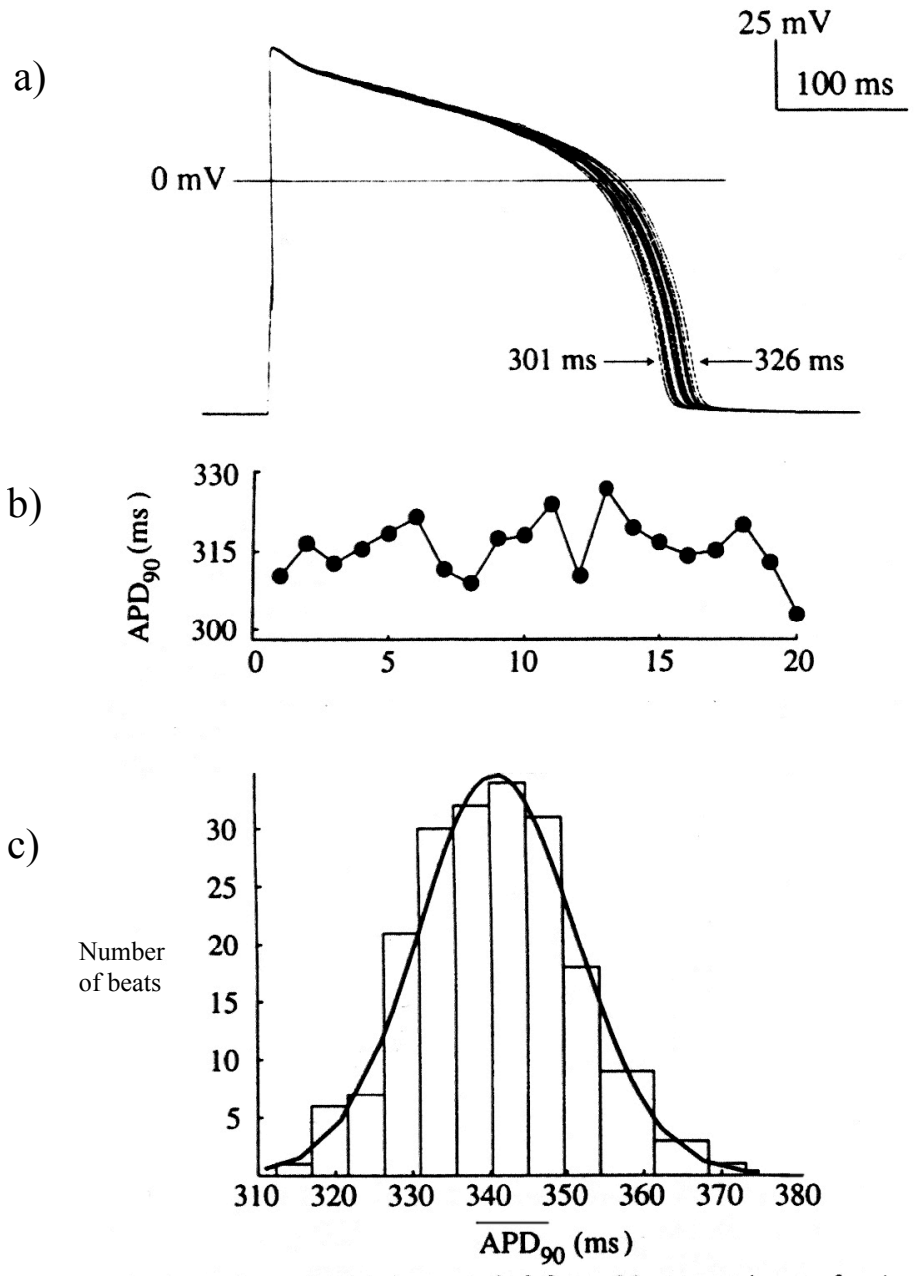

Figure 13. Beat-to-beat APD variability. *a) Action potentials recorded from 20 successive cycles in a single guinea pig ventricular myocytes showed beat-to-beat variability in action potential duration at 90% repolarization (APD_{90}); b) time sequence for APD_{90} in the cell from a; c) histogram of APD_{90} recorded from 200 successive cycles from a different myocytes with Gaussian fit to histogram data (solid line). (From Zaniboni et al, 2000).*

Normal sinus rhythm

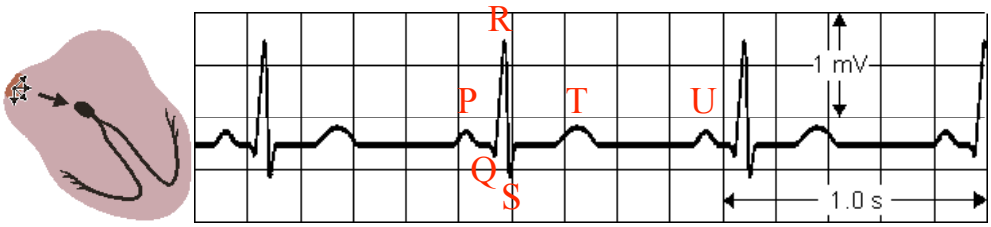

Figure 14. Electrocardiogram (ECG). *The different waves that comprise the ECG represent the sequence of depolarization and repolarization of the atria and ventricles. The ECG is recorded at a speed of 25 mm/sec, and the voltages are calibrated so that 1 mV = 10 mm in the vertical direction.*

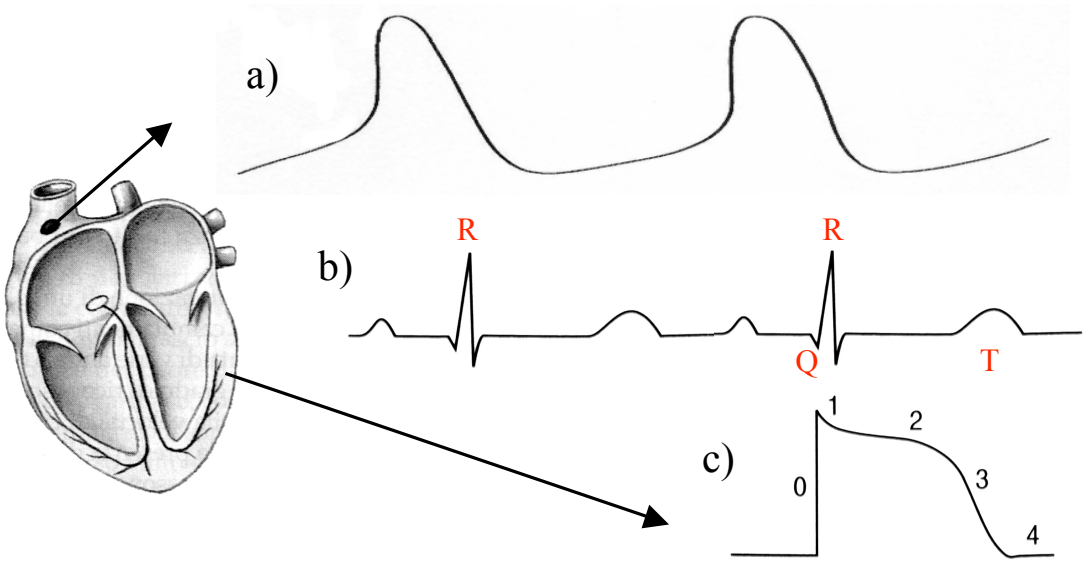

Figure 15. Relation between ECG and AP. *The heart rate and the duration of the excitation are recorded in the electrocardiogram like R-R interval and Q-T duration (b). The R-R interval provides a useful index of the rate of discharge of the nodal pace-maker cells (a). The Q-T interval provides a useful index of the ventricular action potential duration (c).*

Materials and methods

Cell isolation

Single cells were enzymatically isolated from adult (6 months old, 400–500 g) male Wistar rat left ventricles. Each rat was anaesthetized with ether inhalation and killed by decapitation. The heart was rapidly removed, mounted on a Langendorff apparatus (figure 5), and perfused at 37°C with the following sequence of solutions: Ca^{2+}-free (control, no added calcium) Tyrode solution for 5 min to remove the blood, low-Ca^{2+} (0.1mm) solution containing 1mg ml^{-1} type 2 collagenase (Worthington, Lakewood, NJ, USA) and 0.1 mg ml^{-1} type XIV protease (Sigma Aldrich, Milan, Italy) for 20 min, and enzyme-free low-Ca^{2+} solution for 5 min. The left ventricle was then minced and shaken for 10 min in the low-Ca^{2+} solution. Myocytes were stored at room temperature in the control solution with 0.5mM Ca^{2+}. All experiments were performed within 2–8 h after isolation. The procedure was approved by the Veterinary Animal Care and Use Committee of the University of Parma and conformed to the National Ethical Guidelines (Italian Ministry of Health; D.L.vo 116, January 27, 1992).

Solutions

Isolation solution contained (mm): 126 NaCl, 22 dextrose, 5.0 $MgCl_2$, 4.4 KCl, 20 taurine, 5 creatine, 5 sodium pyruvate, 1 NaH_2PO_4 and 24 Hepes (pH adjusted to 7.4 with NaOH). The solution was gassed with 100% O_2. Normal Tyrode solution (NT) for bathing of cells during experiments contained the following (mM): 126 NaCl, 11 dextrose, 5.4 KCl, 1.0 $MgCl_2$, 1.08 $CaCl_2$ and 24 Hepes (pH adjusted to 7.4 with NaOH). In some experiments, NT was added with 5mM of 4-aminopyridine (4-AP), a transient-outward potassium current (I_{to}) blocker, or with 10 μM of nifedipine (from a stock solution in DMSO), an L-type calcium current (I_{CaL}) blocker. The pipette filling solution contained (mm): 113 KCl, 10 NaCl, 5.5 dextrose, 5 K_2ATP, 0.5 $MgCl_2$ and 10 Hepes (pH adjusted to 7.1 with KOH). A drop of storage solution containing cells was placed in the experimental chamber (~2.5 ml) and superfused by gravity at a flow rate of about 2 ml min^{-1}. The temperature of the solutions in the cell

bath was 37°C.

Electrical recordings

Suction pipettes were made from borosilicate capillary tubing (Harvard Apparatus, Edenbridge, UK) and had a resistance, when filled, of 2–4 MΩ. Transmembrane potential (V_m) was recorded by means of an Axoclamp 2B amplifier (Axon Instruments, Union City, CA, USA), adopting the whole-cell configuration of the patch clamp technique (figure 6). Transmembrane potential was digitized at a sampling frequency from 5 to 10 kHz with a 12-bit analog-to-digital converter (Digidata 1200 Series Interface, Axon Instruments). Before a cell was contacted with the pipette tip, the pipette potential was set to zero and the voltage drop across the pipette was compensated with the bridge balance. Action potentials were elicited by means of constant current injections (3 ms, 2–3 nA). The APD was calculated as the interval between the time of maximal upstroke velocity and the time when V_m reached -60 mV ($APD_{-60\ mV}$) and -20 mV ($APD_{-20\ mV}$). When not otherwise specified, mean, standard deviation (S.D.) and coefficient of variability (CV = 100 S.D./mean APD) of APD were calculated over 10 consecutive beats after the AP waveform reached a stable configuration. We used custom-made software written in Matlab (The Mathworks Inc., Natick, MA, USA) to measure these parameters in series of consecutive action potentials. An interpolation procedure over the digitized V_m traces allowed a better time resolution on the raw data acquired at 5 kHz. A program was also written in Matlab language in order to generate randomly changing and linearly changing trigger signals, the first being sequences of trigger signals with CL uniformly distributed within a given percentage (CL_R) of the basic cycle length (BCL) of 250 ms (figure 3), the second being sequences of saw-tooth varying CLs ranging between ±10% or ±20% of 250 ms (figure 4). In addition, trigger signals for constant CL stimulations with pre-/postmature stimuli were first generated in Matlab and then used to drive Axoclamp 2B current injections during the experiment (figure 2). An electronic analog stimulator (Crescent Electronics, Sandy, UT, USA) was used to trigger the amplifier in protocols where switches between two constant values of pacing frequency were applied. In order to minimize the effects of ion depletion and run-down of ionic currents inherent in the whole-cell technique, we checked for the invariance of AP waveform before and after each pacing train and

avoided long stimulation protocols. All experiments were performed within 2 min after establishing the whole cell configuration (individual stimulation protocols never exceeded 8 s), the only exceptions being a few low frequency stimulations (1 and 0.2 Hz) and steady-state rate-dependency experiments, which never lasted more than 5 min. A previous study (Zaniboni *et al.* 2000 and 2005) reported no difference, in terms of beat-to-beat APD variability, between the ruptured patch and the more technically demanding perforated patch; therefore, the latter was not adopted in this study.

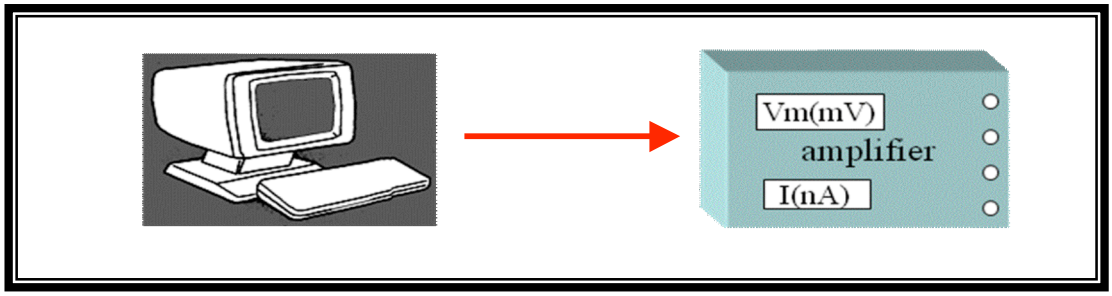

Isolated rat left ventricular myocytes underwent one of the following stimulation protocols:

1

Rate dependency

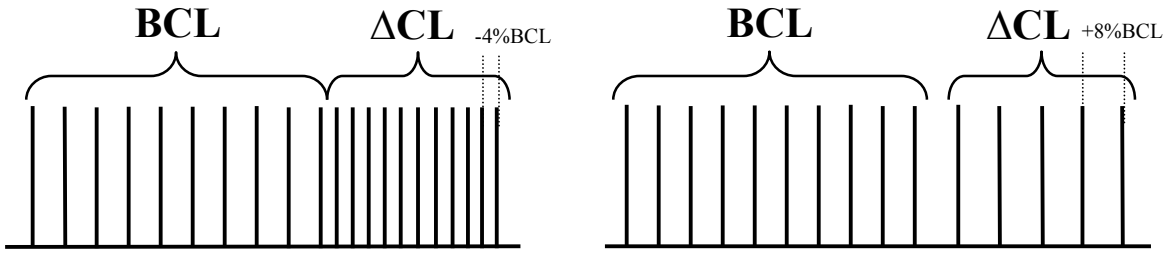

Fig 1. *CL is switched from BCL to different constant CL (up to BCL ±20%) by steps of ±4%*

2

Restitution

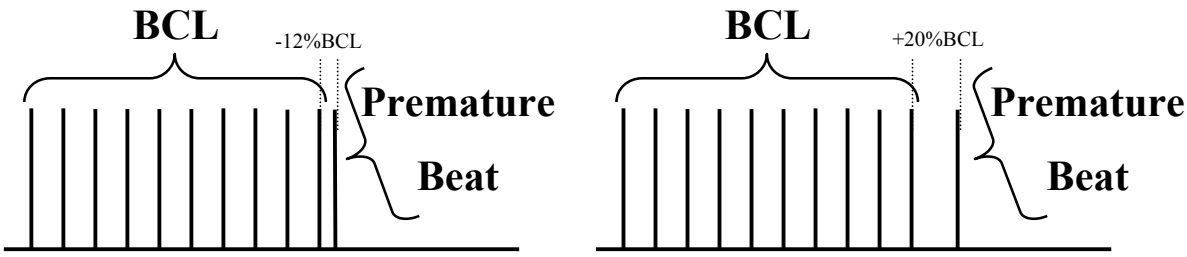

Figure 2. *BCL trains are followed by pre/postmature stimuli with different delays.*

3

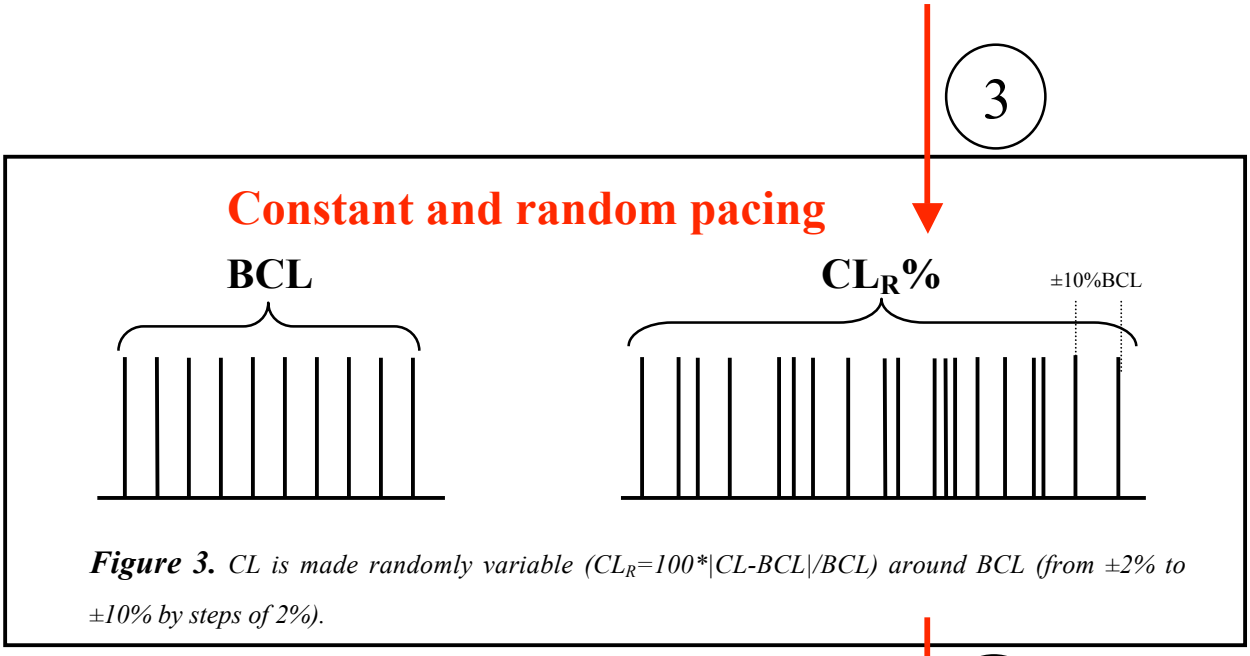

Figure 3. *CL is made randomly variable (CL_R=100*|CL-BCL|/BCL) around BCL (from ±2% to ±10% by steps of 2%).*

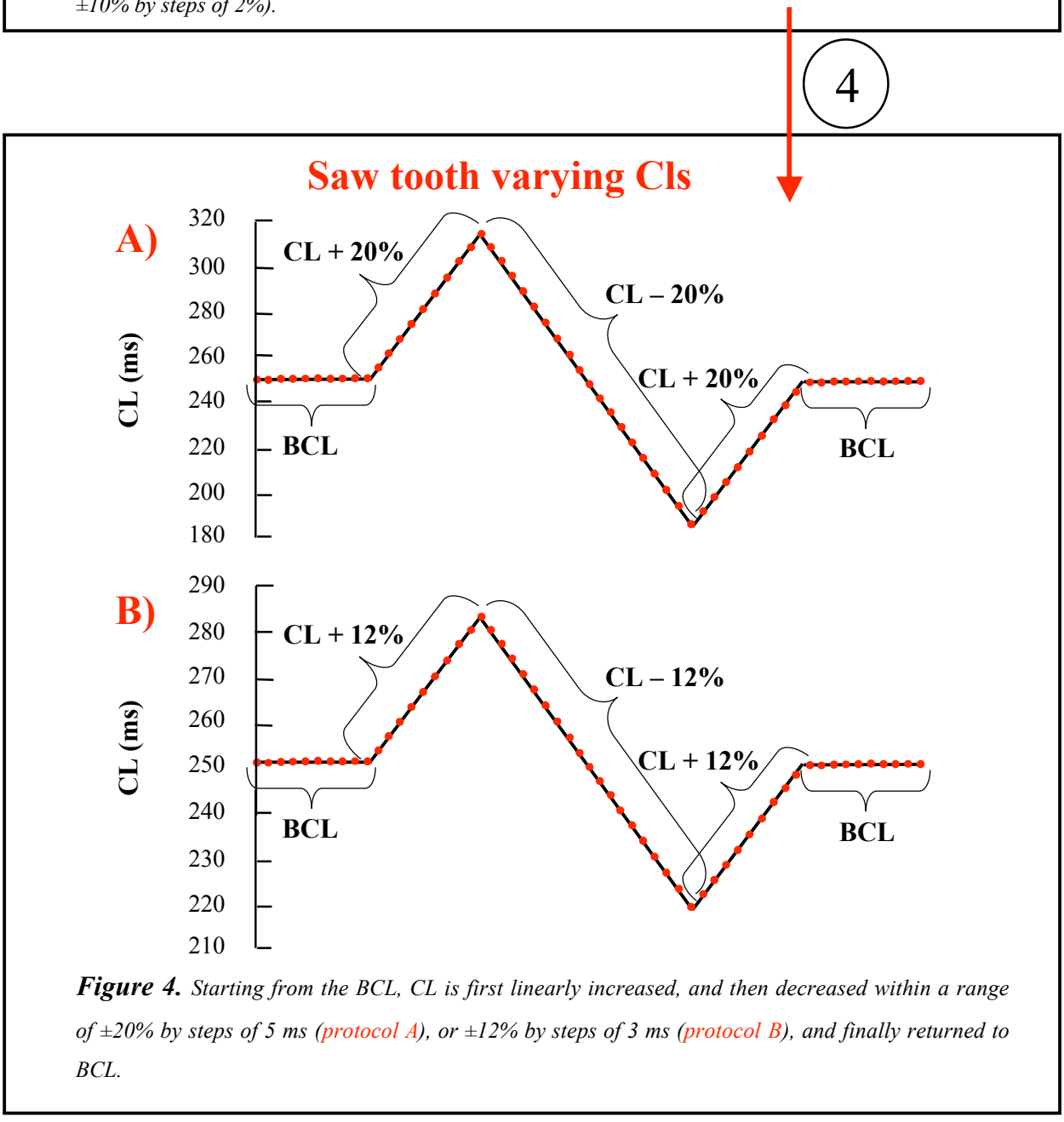

Figure 4. *Starting from the BCL, CL is first linearly increased, and then decreased within a range of ±20% by steps of 5 ms (protocol A), or ±12% by steps of 3 ms (protocol B), and finally returned to BCL.*

Statistics

Results are presented as means ± S.E.M. Student's paired and unpaired *t* tests, one-way ANOVA, as well as Kolmogorov–Smirnov test to check for normality of distributions, were performed by means of SPSS software (SPSS, Chicago, IL, USA). Statistical significance was set at $P < 0.05$. Correlations between $APD_{-60\ mV}$ and CL sequences were performed by means of the 'CORRCOEF' Matlab function on the two vectors.

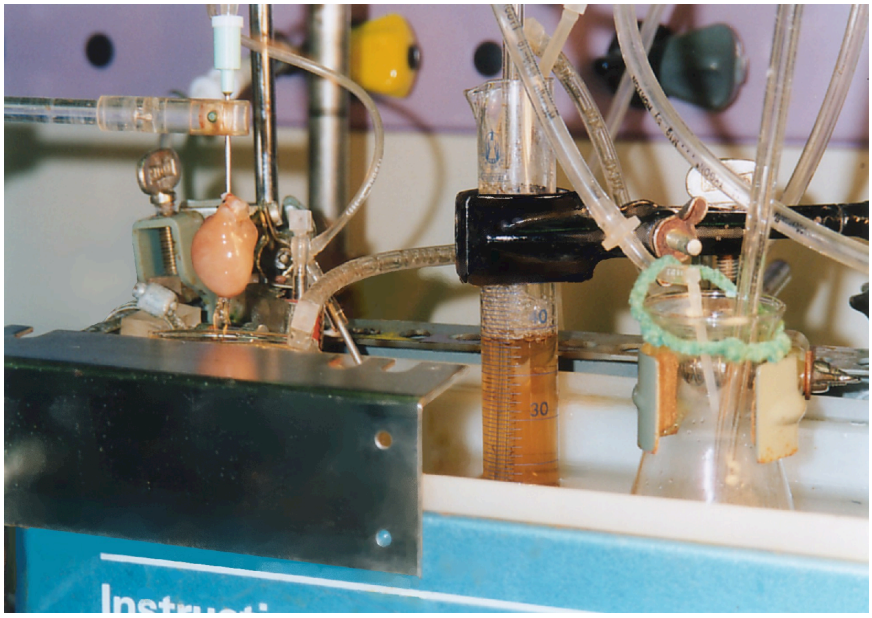

Figure 5. Langerdorff apparatus. Rat heart mounted on Langerdorff apparatus during the perfusion with the isolation solutions.

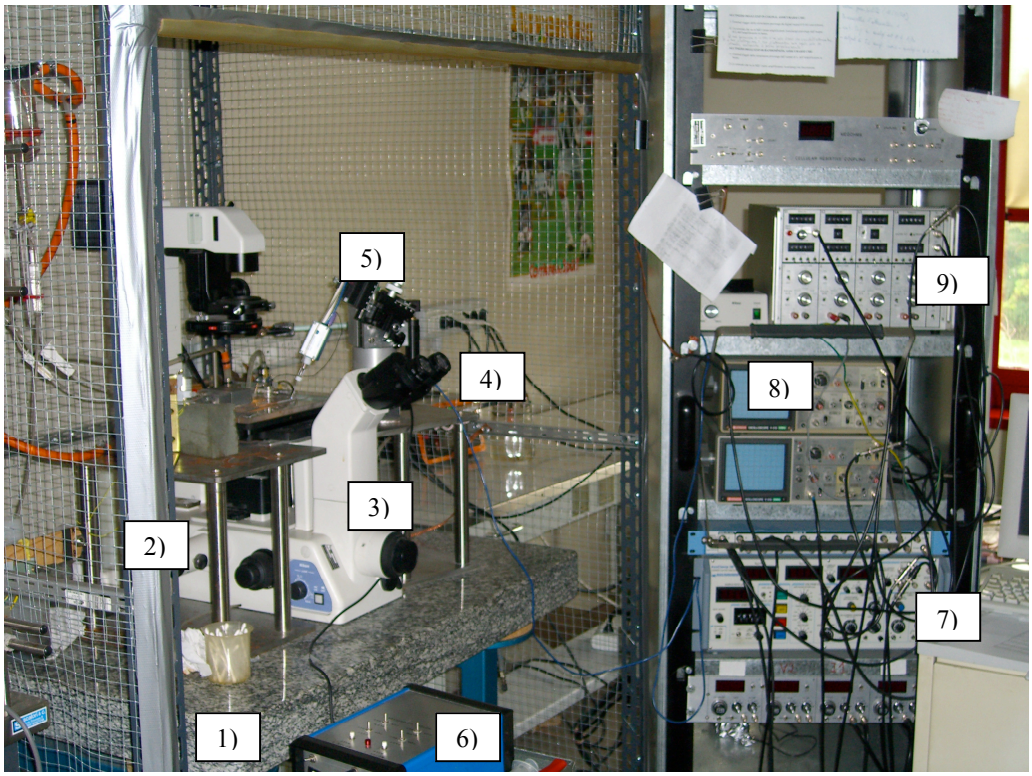

Figure 6. Patch-clamp setup in the cellular electrophysiology laboratory. *Setup is equipped with the following instruments: 1) vibration isolation table; 2) Faraday cage; 3) inverted microscope; 4) pomp for bath perfusion; 5) motorized micromanipulator for recording pipette and 6) controller units for manipulator; 7) patch-clamp amplifier (Axoclamp 2B amplifier; Axon Instruments); 8) oscilloscope; 9) electronic analog stimulator (Crescent Electronics).*

Results and discussion

Beat-to-beat variability of $APD_{-60\ mV}$ was first measured in myocytes electrically stimulated at fixed pacing rates. Figure 1*A* shows beat-to-beat changes of $APD_{-60\ mV}$ over several cycles of a cell paced at 1 Hz. Longer stimulations allowed analysis of frequency distribution in terms of Gaussian fits for series of $APD_{-60\ mV}$ recorded in the same cell at three different pacing rates (Fig. 1*B*). All the distributions were normal (Kolmogorov–Smirnov test: $P = 0.77$ for 5 Hz; $P = 0.95$ for 1 Hz; and $P = 0.5$ for 0.2 Hz), which suggests, although without proving it, a random origin for the process. Increasing the pacing rate brought about a significant (one-way ANOVA, $P < 0.05$) decrease in S.D. $_{-60\ mV}$ (from 3.50 ms at 0.2 Hz to 1.31 ms at 5 Hz) and $CV_{-60\ mV}$ (Fig. 5*C*). This effect was also studied in a larger group of cells ($n = 100$) which were paced at only two frequencies and where a highly significant ($P < 0.01$) decrease in S.D. $_{-60\ mV}$ (from 2.33 to 1.37 ms) and $CV_{-60\ mV}$ (from 2.55 to 1.37%) was found when pacing rate was increased from 1 to 5 Hz. Figure 5*D* emphasizes the overall changes of $APD_{-60\ mV}$ range and $APD_{-60\ mV}$ variability with increasing pacing rate, as well as the increase in temporal dispersion with increasing intrinsic $APD_{-60\ mV}$. We note that rate-dependent shortening of APD was not a consistent finding in our pacing experiments, where in fact a minority of the entire cell population (2 out of the 9 cells of Fig. 1*C*), unspecifically isolated from the entire left ventricle, showed $APD_{-60\ mV}$ rate dependent prolongation but a similar rate dependency of $CV_{-60\ mV}$. The two groups of myocytes, unambiguously identified from the positive or negative slope of their $APD_{-60\ mV}$ rate dependency, did not significantly differ in resting membrane potential (~ –75 mV), action potential amplitude (~ 93 mV) and $APD_{-60\ mV}$ (~ 87 ms, measured at a BCL of 250 ms). We further characterized beat-to-beat $APD_{-60\ mV}$ variability at a BCL of 250 ms, which is comparable to the rat physiological sinus rhythm. Figure 2*A* shows $APD_{-60\ mV}$ -dependent increase of $S.D._{-60\ mV}$ for cells perfused in NT, in 10 μM nifedipine or in 5 mM 4-AP. In control conditions, for example, shorter values of $APD_{-60\ mV}$ (~ 50 ms) ranged ±3ms (±3 S.D.), whereas longer values of $APD_{-60\ mV}$ ranged up to ±9 ms. Nifedipine, as expected, shortened the entire $APD_{-60\ mV}$ range, whereas 4-AP slightly prolonged it, none of the treatments producing a significant change in the S.D. $_{-60\ mV}$ range for the entire cell population. Overall drug-induced differences in beat-to-beat $APD_{-60\ mV}$

variability became significant when measured as S.D. $_{-60\ mV}$ normalized to mean $APD_{-60\ mV}$ ($CV_{-60\ mV}$), as shown in the frequency distributions of Fig. 2*B*. Nifedipine significantly increased the average $CV_{-60\ mV}$ value, whereas 4-AP reduced the same parameter.

Action potential duration rate dependency and electrical restitution properties

In order to estimate how beat-to-beat APD variability will limit the detection of rate-dependent effects on cellular repolarization, we performed two classical stimulation protocols. Steady-state rate dependency of $APD_{-60\ mV}$ was quantified for small (<±20%) changes (ΔCL) in BCL. Cells were paced for ~13 s at a BCL of 250 ms, which was suddenly switched to different constant values, allowing each time for the action potential to reach a new steady-state configuration (~ 100 beats). It appears (Fig. 3*A*) that steady-state rate-dependent APD changes for |ΔCL| = 4% fell very close to the average intrinsic beat-to-beat variability range of $APD_{-60\ mV}$ (hatched horizontal region), and only higher ΔCLs were likely to be detected in terms of stable changes in recovery time. In Fig. 3*B* we report results of experiments on electrical restitution where only the last 10 conditioning beats at a BCL of 250 ms and a pre-/postmature test beat were measured. Since the test stimulus is the equivalent of the first stimulus at a new pacing rate, and for homogeneity with Fig. 3*A*, we refer to it, on the abscissa, as a new CL value. Instantaneous AP sensitivity to sudden changes of CL appeared to be asymmetric, where sudden prolongations of CL were sensed more, in terms of $APD_{-60\ mV}$, than sudden shortenings. Even very small increases in CL of only 4% were in fact detected, on average, as measurable (larger than beat-to-beat variability) $APD_{-60\ mV}$ prolongations, whereas only considerable decreases (>12%) were detected as measurable $APD_{-60\ mV}$ shortenings. A minority of cells (n = 4 for the rate-dependency experiments and n = 3 for the restitution experiments) showed rate-dependent $APD_{-60\ mV}$ prolongation and a negative sloping restitution curve. The corresponding data, comparable in amplitude of changes but with opposite sign, are reported in Fig. 3C.

Beat-to-beat APD variability in random-frequency stimulations

Beat-to-beat variability of $APD_{-60\ mV}$ ($CV_{-60\ mV}$) was measured in myocytes perfused

in NT and electrically stimulated, initially at a BCL of 250 ms (CL_R = 0%), and subsequently with randomly variable CL trains with progressively increased degree of randomness (CL_R, see Methods; Fig. 4). The average $CV_{-60\ mV}$ value measured at CL_R = 0% (dashed horizontal line) did not change significantly until CL_R reached 6%, where it started to increase with the increasing of CL_R. Some of the cells underwent the same protocol after drug exposure (not shown except for the data at CL_R = 0% reported in Fig. 2). Nifedipine significantly increased $CV_{-60\ mV}$ at almost all values of CL_R (+30% on average), whereas 4-AP decreased it (–24% on average).

Correlation between $APD_{-60\ mV}$ and CL for random fluctuations of CL: a 'random restitution' curve

Figure 5 reports scatter graphs for several superimposed 10-beat random stimulations (CL_R =10%) of $\Delta APD_{-60\ mV}$ values *versus* preceding CL (we will call them briefly 'random restitution curve'). It appears that the increased variability in $APD_{-60\ mV}$ measured at CL_R = 10% in NT (Fig. 4) was not random, but tended to correlate positively with beat-to-beat changes in CL (average correlation coefficient, r = 0.43; single statistically significant coefficients were 11 out of 21; slope = 0.04% ms^{-1}). In other words, a beat-to-beat shortening of the preceding CL tended to make APD shorter, and vice versa for a beat-to-beat prolongation of CL (see also the time sequence in the insets of Fig. 5*A*, *B* and *C*). Random stimulations in NT with higher CL_R (20%) reached higher correlation (r = 0.71; single statistically significant coefficients were 10 out of 13; and slope = 0.06% ms^{-1}, not shown). Nifedipine-induced shortening of APD tended to abolish this correlation (r = 0.23; none of the single coefficients was statistically significant; slope = 0.03% ms^{-1}), whereas 4-AP-induced prolongation brought it up to statistical significance (r = 0.67; single statistically significant coefficients were 7 out of 9; slope = 0.06% ms^{-1}; see Fig. 5*B*, *C* and *D*). Analogous behavior was found when restitution was measured as $\Delta APD_{-60\ mV}$ *versus* preceding DI (NT, positive slope with r = 0.48; nifedipine, r = 0.22; 4-AP increased slope with r = 0.62).

Correlation between $APD_{-60\ mV}$ and CL for linearly changing CL

The property of nifedipine and 4-AP of, respectively, uncoupling and coupling $APD_{-60\ mV}$ with the preceding CL was further demonstrated with saw-tooth pacing

protocols ranging ±10 and ±20% of a BCL of 250 ms (Fig. 6). With the ±10% protocol, $APD_{-60\ mV}$ usually tended to correlate positively with monotonically changing preceding CL (r = 0.45), nifedipine dramatically reduced this correlation (R= –0.04), whereas 4-AP significantly increased it (r = 0.80; Fig. 10*A*). Analogous results were obtained with ±20% ramps (Fig. 6*B*, *C* and *D*). A tendency for rate-dependent $APD_{-60\ mV}$ prolongation in NT was found in only two myocytes of those subsequently perfused with 4-AP and two of those subsequently perfused with nifedipine, which were not included in the previous statistic. We note, however, that in those cases the exposure to the blockers also led to a significant positive correlation in the case of 4-AP (r = 0.70) and a to loss of correlation (R = –0.31) in the case of nifedipine.

Measurements of APD during early repolarization

All measurements reported in this study for $APD_{-60\ mV}$ have also been performed for $APD_{-20\ mV}$. Briefly, at CL_R = 0%, $APD_{-20\ mV}$ always (in NT, nifedipine and 4-AP) correlated with $APD_{-60\ mV}$ (r = 0.67 on average) over 10- beat sequences. $CV_{-20\ mV}$ was much greater than $CV_{-60\ mV}$ (twice on average) and prevented the detection of classical rate-dependent and restitution properties within a CL range of ±10%. No significant drug- or rate-induced difference was measurable at $CV_{-20\ mV}$, nor could any drug-induced difference be assessed in the $APD_{-20\ mV}$ – CL correlation during randomly or linearly changing CL protocols.

Discussion

Our findings on temporal dispersion of APD in rat ventricular myocytes can be summarized as follows. First, intrinsic beat-to-beat dispersion of repolarization increases with intrinsic APD and, when normalized to it, is inversely proportional to pacing frequency, increased by nifedipine and decreased by 4-AP. Second, both random and linear changes in pacing CL, even the smallest detectable in repolarization (larger than intrinsic beat-to-beat variability), tend to correlate positively with APD changes. Finally, nifedipine abolishes this correlation, uncoupling APD from the preceding CL, whereas 4-AP increases correlation, coupling the time course of the two parameters over consecutive beats. Zaniboni *et al.* (2000) reported a CV of 2.3% for the beat-to-beat APD variability of guinea-pig

ventricular myocytes paced at 0.5 Hz. This fits with the $CV_{-60\ mV}$ *versus* CL relationship we illustrate in Fig. 5*C* for rat myocytes, although measurements in the present study have been performed in terms of $APD_{-60\ mV}$ (see Methods) instead of APD at 90% of repolarization. Our additional attempt to measure temporal dispersion of APD in the early phase of repolarization leads us to conclude that the variability of $APD_{-20\ mV}$, although qualitatively reproducing the variability of $APD_{-60\ mV}$ (they are correlated), is a less appropriate parameter to detect beat-to-beat repolarization changes in this cell type.

Also in accordance with the cited guinea-pig study, longer rat ventricular APDs are found to be more temporally dispersed. We show here, for the first time, that this relationship holds at different pacing rates (Fig. 1*D*) and for different pharmacological treatments (Fig. 2*A*), and we suggest in the Appendix an explanation for this effect, based on the resistive properties of the cell membrane during repolarization. While the increase of heart rate does not induce detectable changes in the dispersion of endocardial monophasic APD in dogs and humans (Hirao *et al.* 1996; Zabel *et al.* 1997), it is found to significantly decrease the increased dispersion of APD in long QT syndrome patients with pathologically prolonged action potentials, supporting the efficacy of pacemaker therapy to decrease propensity for arrhythmia (Hirao *et al.* 1996). The present study shows, for the first time, that the rate dependency of APD variability, measured as either $S.D._{-60\ mV}$ or $CV_{-60\ mV}$ (Fig. 1*C* and *D*), is intrinsically present in the isolated cardiomyocyte also in non-pathological conditions, in the absence of higher level controls (e.g. electrotonic interactions, autonomic modulation, spatial sequence of activation) which operate within the whole organ. Cellular beat-to-beat APD variability and its APD dependency and rate dependency are not likely to be critical within the tissue in normal conditions, where temporal dispersion is reduced by electrotonic interactions (Zaniboni *et al.* 2000). In contrast, junctional uncoupling can unmask intrinsic beat-to-beat variability of APD, leading to a substrate more prone to unidirectional block and re-entry (Lesh *et al.* 1989). It is in this context that the intrinsic APD dependency and rate dependency of beat-to-beat repolarization variability might contribute to the initiation of arrhythmic events, especially in those pathologies (e.g. heart failure), or in ageing, which simultaneously decrease intercellular coupling and sinus rhythm, while increasing APD (Janse, 2004; Severs *et al.* 2004). Our further finding that intrinsic APD variability at a BCL of 250 ms increases only for random changes of

CL greater than 4% (Fig. 4) and tends to correlate with them on a beat-to-beat basis (Fig. 5), has not been shown previously in isolated ventricular myocytes. A ~ 50% rise of CV of APD, secondary to a rise in CV of CL (from 2.3 to ~5%), has been reported by Rocchetti *et al.* (2000) in a different cell type (spontaneously beating sinoatrial myocytes) following acetylcholine application, while a correlation between the RT segment of ECG and the preceding CL, although for much larger random CL changes, has been found in dogs (Lux & Ershler, 2003). The range we chose for CL variability (2–10%, some experiments at 20%) during rate-varying stimulations is comparable with beat-to-beat oscillations of rat sinus rhythm, which are reported to be around 4% in normal resting conditions, and to vary physiologically between 2 and 8%, for example during and following episodes of social stress (Sgoifo *et al.* 1998); vagal recruitment can bring these values to even higher physiological levels (Schipke & Pelzer, 2001; Hautala *et al.* 2001). Based on previous findings that showed a differential contribution of different ion channels to beat-to-beat APD variability (Zaniboni *et al.* 2000), we wanted to test the relative contribution of I_{CaL} and I_{to}, major determinants of membrane repolarization and restitution properties of rat cardiomyocytes (Nanasi *et al.* 1996; Janvier *et al.* 1997), in mediating interbeat APD variability during constant pacing rate and in modulating APD–CL correlation during randomly/linearly changing pacing rate. Nifedipine and 4-AP, together with their known shortening/prolonging effect on ventricular AP, brought about an overall increase/decrease in beat-to-beat APD variability (Fig. 2) which cannot be derived from the argument in the Appendix and seems to be related, instead, to the different extent of interbeat stochastic changes in the amount of I_{CaL} and I_{to} flowing during the course of an action potential. The picture is consistent with (1) an I_{CaL} endowed with a stabilizing effect on repolarization which is achieved by coupling APD with preceding CL, most likely through residual voltage- and calcium-dependent inactivation and through intermediate steps of calcium handling, (2) an I_{to} acting as a source of random changes on AP trajectory, uncoupling APD from preceding CL. Therefore, nifedipine-induced APD shortening allows more time for diastolic recovery of both ion channels from inactivation and resetting of calcium handling mechanisms, unmasking beat-to-beat random changes of I_{to} at constant pacing rate (Fig. 2*B*) and uncoupling each APD from the preceding CL (loss of correlation), in both randomly and linearly changing pacing protocols (Figs 5 and 6). Conversely, 4-AP decreases the source of interbeat random changes of APD at constant pacing rate

(Fig. 2*B*) and, by shortening the diastole, prevents complete removal of inactivation processes and resetting of calcium handling mechanisms, coupling each APD with the preceding CL during rate-varying stimulations (higher correlation; Figs 5 and 6). Both blockers, by uncoupling APD from the preceding beat and by reducing the ionic source of interbeat stochastic changes, respectively, overbalance the intrinsic APD dependency of APD variability. A direct effect of these blockers on intrinsic beat-to-beat variability of APD has not been shown previously and is of interest, given that one of the beneficial effects of anti-arrhythmic drugs is thought to be their ability to decrease temporal dispersion of repolarization in the heart (Kuo *et al.* 1983; Fynn *et al.* 2003). We note that the mechanism we propose for the involvement of I_{CaL} and I_{to} in APD variability is also consistent with the rate dependency of CV. In fact, an increase of the pacing frequency from 0.5 to 3 Hz is reported to decrease I_{to} by more than 50% in rat ventricular myocytes (Pandit *et al.* 2001), meanwhile reducing I_{CaL} by only 30% (McMorn *et al.* 1998). In other words, increasing the pacing rate will have a greater impact in reducing random changes of I_{to} during early repolarization, resulting in an overall decrease of CV_{-60mV}. Premature beats frequently initiate ventricular arrhythmias in ischaemic conditions (Janvier *et al.* 1997), and electrical restitution provides a tool for predicting such events (Franz, 2003). Nifedipine has been reported to decrease, and 4-AP to increase, the slope of the restitution curve, both in single cells, although at non-physiological pacing rates (Nanasi *et al.* 1996; Janvier *et al.* 1997), and in tissue preparations, where the pharmacologically induced slope reduction has been proposed to prevent oscillations of APD which lead to development of VF (Riccio *et al.* 1999). Our work shows, for the first time, that this effect of nifedipine and 4-AP can be measured at the cellular level in physiologically dynamic pacing conditions, where the slope of the corresponding random restitution curve (Fig. 5*A*) is comparable with that of classical restitution within the same CL range. This could not be simply predicted from classical rate-dependent and restitution properties, since these are measured at the steady state of membrane excitability and calcium handling, which is never achieved in dynamic conditions. A random pacing approach to cellular restitution might therefore represent a suitable model for further exploration of the intrinsic cellular counterpart of the more complex dynamic restitution of the heart.

Limitations of the study

An intrinsic limitation with any pharmacological block of specific ion channels in current clamp experiments is that AP waveform undergoes changes which in turn modify the relative contribution of all the ionic currents involved in repolarization. The mechanism we propose for the 4-AP and nifedipine effect on APD variability, based on stochastic contribution of only two ionic currents, does not rule out the possible involvement of other currents secondarily affected by the block, although it coherently explains all the data presented. Simulations by means of mathematical models of the rat ventricular action potential (Pandit *et al.* 2001), including controlled sources of variability, would be of interest at this regard. Also, we did not investigate the possibility that other mechanisms, such as those involved in intracellular calcium dynamics, or other ion channels involved in electrical restitution (e.g. delayed rectifier K^+ current (I_K), Na^+-Ca^{2+} exchange current (I_{NaCa}); Janvier *et al.* 1997) would play some role in APD variability at constant pacing or in APD–CL correlation during randomly and linearly changing pacing rates. Finally, the rat ventricle, although widely used as an experimental model for the study of electrical heterogeneity in normal and pathophysiological conditions (see references in the Introduction of the paper by Pandit *et al.* 2001), has a peculiar AP profile (lacking plateau) and rate-dependent properties (Shigematsu *et al.* 1997; Carmeliet, 2006), which call for caution in extrapolating our results to other mammals and, in particular, to humans. A complication arises from the expected finding, together with rate dependent APD shortening myocytes, of rate-dependent APD prolonging myocytes, owing to spatial heterogeneity in repolarization properties and differences in intracellular buffering conditions (Watanabe *et al.* 1983; Shipsey *et al.* 1997; Shigematsu *et al.* 1997; Fauconnier *et al.* 2003). These latter cells (between 22 and 40% in our experiments), unambiguously identified from the negative slope of their restitution curve, did not, however, show differences in the rate dependency of their beat-to-beat $APD_{-60\ mV}$ dispersion, in the absolute value of rate-dependent and classical restitution changes, or in the pharmacological response during linearly CL-varying stimulations.

Appendix

Our results show that myocytes, unspecifically isolated from the entire rat left

ventricular free wall, show a broad range of $APD_{-60\ mV}$ (from 40 to 150 ms), in which the shorter waveforms show smaller S.D. $_{-60\ mV}$ and the longer higher (Fig. 2*A*). This trend holds when APDs are collectively shortened with nifedipine or lengthened with 8-AP. In this Appendix we suggest a possible explanation based on simple calculations on experimental traces. We consider the four representative APs (Vm (t)) of Fig. 7*A* (continuous lines) which span the entire $APD_{-60\ mV}$ range. We then calculate the total ionic current (I_{tot}) flowing during each AP repolarization as:

$$i_{tot}(t) = -C_m\ (dV_m\ (t)/\ dt\ )$$

and report it in the same figure (dotted lines) as a function of membrane potential (I–V relationship). Capacitance values (C_m), as measured with standard DC method (Zaniboni *et al.* 2005), were fairly homogeneous in the four cells, ranging 172±5 pF. We note that, looking at the I–V relationships, the different APs differ remarkably for what concerns membrane ionic current flowing during the early repolarization phase, whereas the second part of repolarization is characterized by an almost identical I–V profile. In fact, the initial part of repolarization, down to ~ –40 mV, is characterized, in each waveform, by a fairly constant membrane slope conductance, whose average value we derived from linear fit to the curves over this region. Average R_m (inverse of conductance) increases with the associated APD (Fig. 7*B*), since the relationship is quasi-linear for $APD_{-60\ mV}$ up to ~90 ms and then diverges for longer waveforms. We note incidentally that R_m during early repolarization of AP1 is identical to that of the resting membrane (~40 MΩ, inverse slope of dashed line, Fig. 7*B*), which is in accordance with recently published DC estimates in the same cell type (Zaniboni *et al.* 2005). We suggest that the increase of early repolarization-R_m with increasing APD can be the source of the relationship between S.D. $_{-60\ mV}$ and mean $APD_{-60\ mV}$ of Fig. 2*A*. Accordingly, longer AP waveforms will have an early repolarization phase characterized by a higher R_m, whereas shorter APs will have a lower resistance. Even in the simplified assumption that each action potential waveform will experience the same random electrical disturbances (the product of beat-to-beat changes in membrane ionic current resulting from stochastic behaviour of the channels and the instantaneous value of R_m) during the time in which most of the repolarization ionic current flows (early repolarization), shorter APs will deviate their interbeat trajectory to a smaller extent (smaller S.D. of APD) than longer APs.

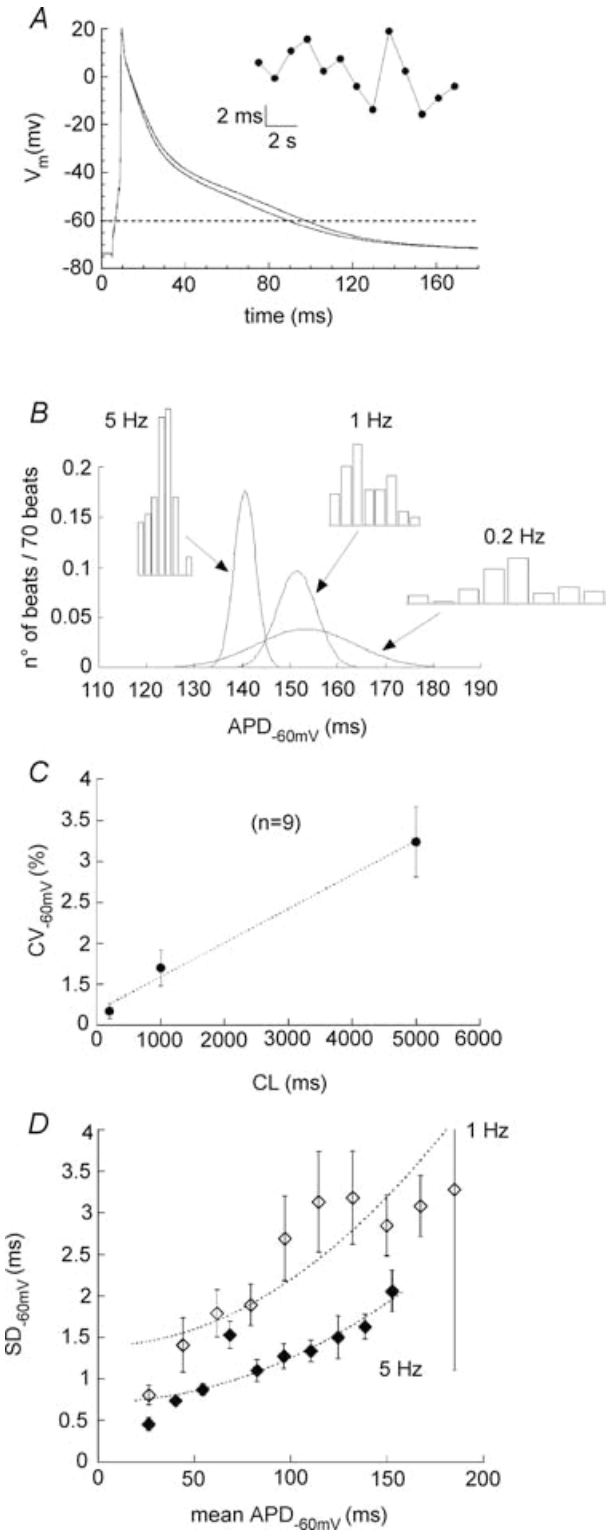

Figure 1. Beat-to-beat APD variability: rate dependency. *A, shortest and longest of 13 consecutive action potentials recorded from an electrically paced (1 Hz) rat ventricular myocyte. Inset shows the corresponding time course of* $APD_{-60\ mV}$. *B, frequency distributions for 70-beat sequences of* $APD_{-60\ mV}$, *recorded from another cell, at three different pacing rates with corresponding Gaussian fits (continuous lines). C,* $CV_{-60\ mV}$ *(*$S.D._{-60\ mV}$ *normalized to mean* $APD_{-60\ mV}$*), as measured from 10-beat sequences in cells which underwent consecutive stimulation protocols at 0.2, 1 and 5 Hz. D, 100 myocytes were paced first at 1 and then at 5 Hz. Mean values of* $APD_{-60\ mV}$ *mV and* $S.D._{-60\ mV}$ *were calculated for each cell; for the sake of clarity, data were pooled and averaged in 10 equally spaced* $APD_{-60\ mV}$ *mV subgroups. Superimposed curves are parabolic fittings in order to emphasize the overall behaviour graphically.*

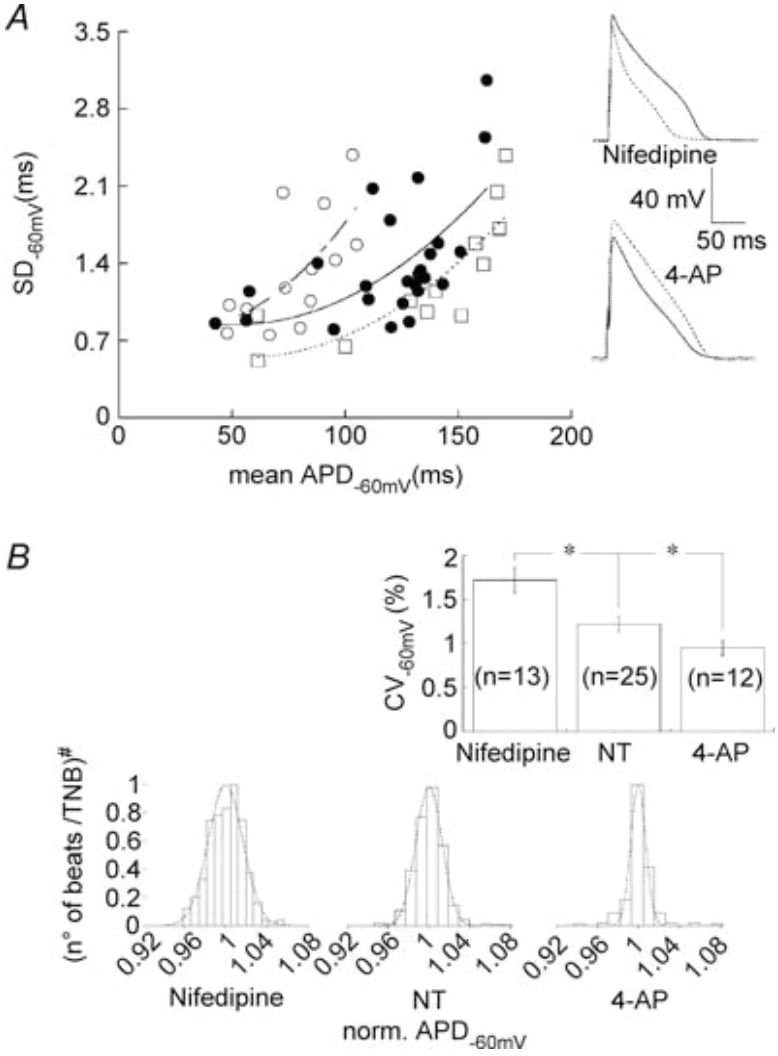

Figure 2. Effect of nifedipine and 4-AP on temporal dispersion of $APD_{-60\ mV}$

*A, beat-to-beat $APD_{-60\ mV}$ variability ($S.D._{-60\ mV}$) for 25 cells in NT (•), 13 cells in nifedipine (○) and 12 cells in 4-AP (□). Measurements in NT are pooled controls from the nifedipine and 4-AP experiments. Each point represents $S.D._{-60\ mV}$ of a 10-beat sequence versus the corresponding mean $APD_{-60\ mV}$ for one cell paced at a BCL of 250 ms. Superimposed curves are parabolic fittings to emphasize the S.D. increase with APD graphically. Inset shows representative examples of the effect of ion channel blockers (dotted lines) on AP waveforms at a BCL of 250 ms, compared with controls (continuous lines). B, frequency distributions for all the 10-beat sequences shown in A; the total number of beats (TNB) was 130 for nifedipine, 250 for NT and 120 for 4-AP. In order to allow comparison between Gaussian fits, ordinates are normalized to 1 (#), and abscissa to mean $APD_{-60\ mV}$ value over each 10-beat sequence. Inset shows statistics of $CV_{-60\ mV}$ for the same data (*P < 0.05).*

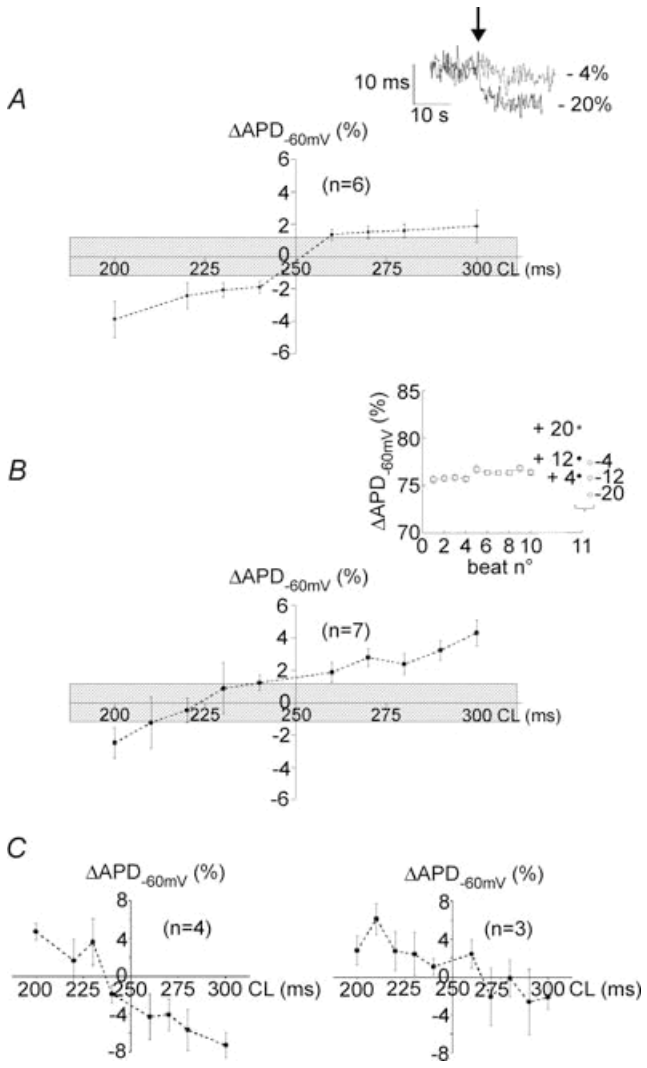

Figure 3. Rate dependency and electrical restitution of $APD_{-60\ mV}$

Rate dependency: 10 cells were paced first at a BCL of 250 ms, which was switched, in turn, to BCL ± m%BCL (m = 4, 8, 12 and 20). Percentage differences between average $APD_{-60\ mV}$ value measured at a BCL of 250 ms and once $APD_{-60\ mV}$ reached a steady state at the new CL, are reported in A as a function of CL for 6 cells which showed rate-dependent $APD_{-60\ mV}$ shortening (slope = 0.065% ms^{-1} from linear fit to the data). Inset shows representative time course of $APD_{-60\ mV}$ during switches (arrow) to 240 and 200 ms on the same cell. Restitution: 10 cells were paced for a few seconds at a BCL of 250 ms, which was suddenly switched (test), in turn, to BCL ± m%BCL (m = 4, 8, 12, 16 and 20). Percentage APD changes between the average value over the last 10 conditioning beats and the test beat are reported in B as a function of CL for 7 cells which showed a positive sloping restitution curve (slope = 0.059% ms^{-1} from linear fit to the data). Inset shows a representative example of six conditioning trains (averaged) followed by corresponding test beats. Only test beats to ±4, ±12 and ±20% are shown, for clarity. In both panels, the shaded area represents the average $APD_{-60\ mV}$ variability range ($\pm CV_{-60\ mV}$) measured in NT at a BCL of 250 ms, as reported in Fig. 6B. C, same as A and B, respectively, for 4 cells which showed rate-dependent $APD_{-60\ mV}$ prolongation (left) and for 3 cells which showed negative sloping restitution curve (right).

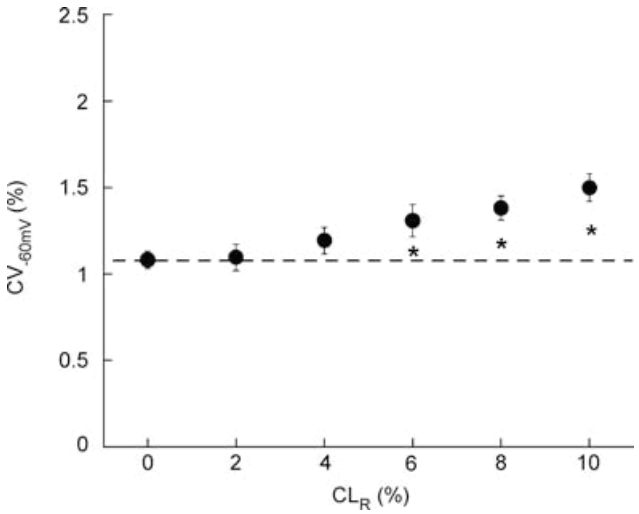

Figure 4. Relationship between beat-to-beat variability of $APD_{-60\ mV}$ and CL_R

*Each of 54 cells was consecutively paced by means of six random-CL protocols with increasing degree of randomness (CLR). Each point represents the average variability of $APD_{-60\ mV}$, over all the cells, for a certain value of CLR, as measured over the last 10 beats of each 32-beat train (*P < 0.05 with respect to CLR = 0%).*

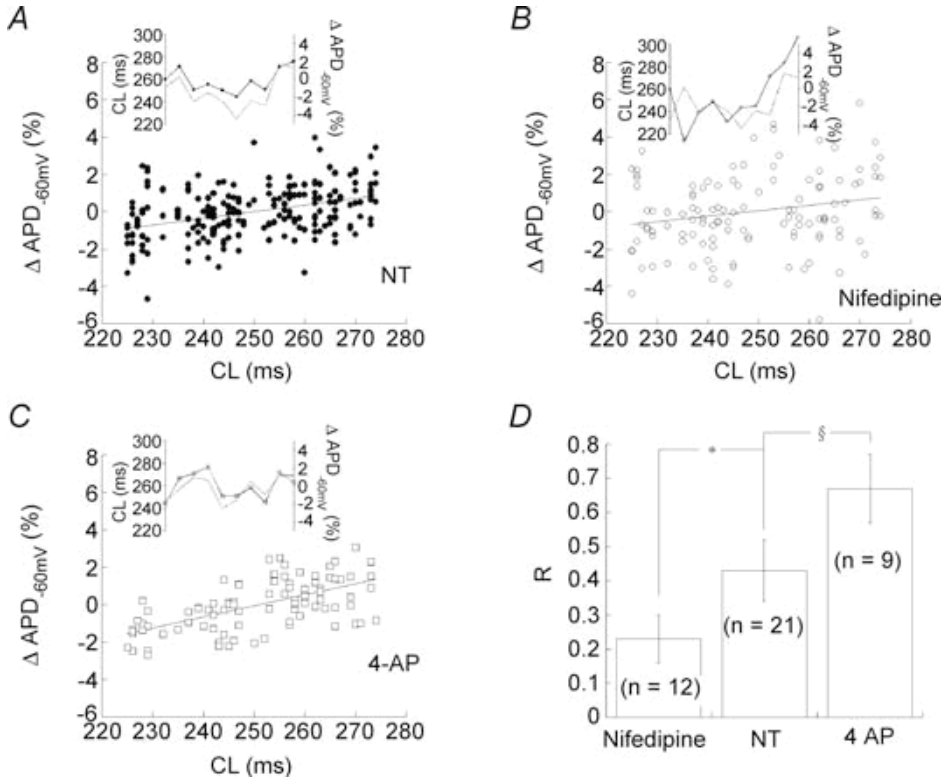

Figure 5. Correlation between $APD_{-60\ mV}$ and randomly changing CL

*A, superimposed 10-beat sequences of APD_{-60mV} (percentage changes from the average value over the 10 beats) versus the preceding CL, of cells paced in NT with a randomly changing CL (CLR = 10%). Inset shows corresponding representative example of a 10-beat sequence of normalized $APD_{-60\ mV}$ (continuous line, each filled circle is 1 beat) and CL (dotted line). B and C, same representation for cells exposed to nifedipine and 4-AP. Continuous lines represent linear fits to the data. D, bar graph with the average correlation coefficients (R) for the APD–CL sequences reported in A, B and C (*P < 0.05; §P = 0.06).*

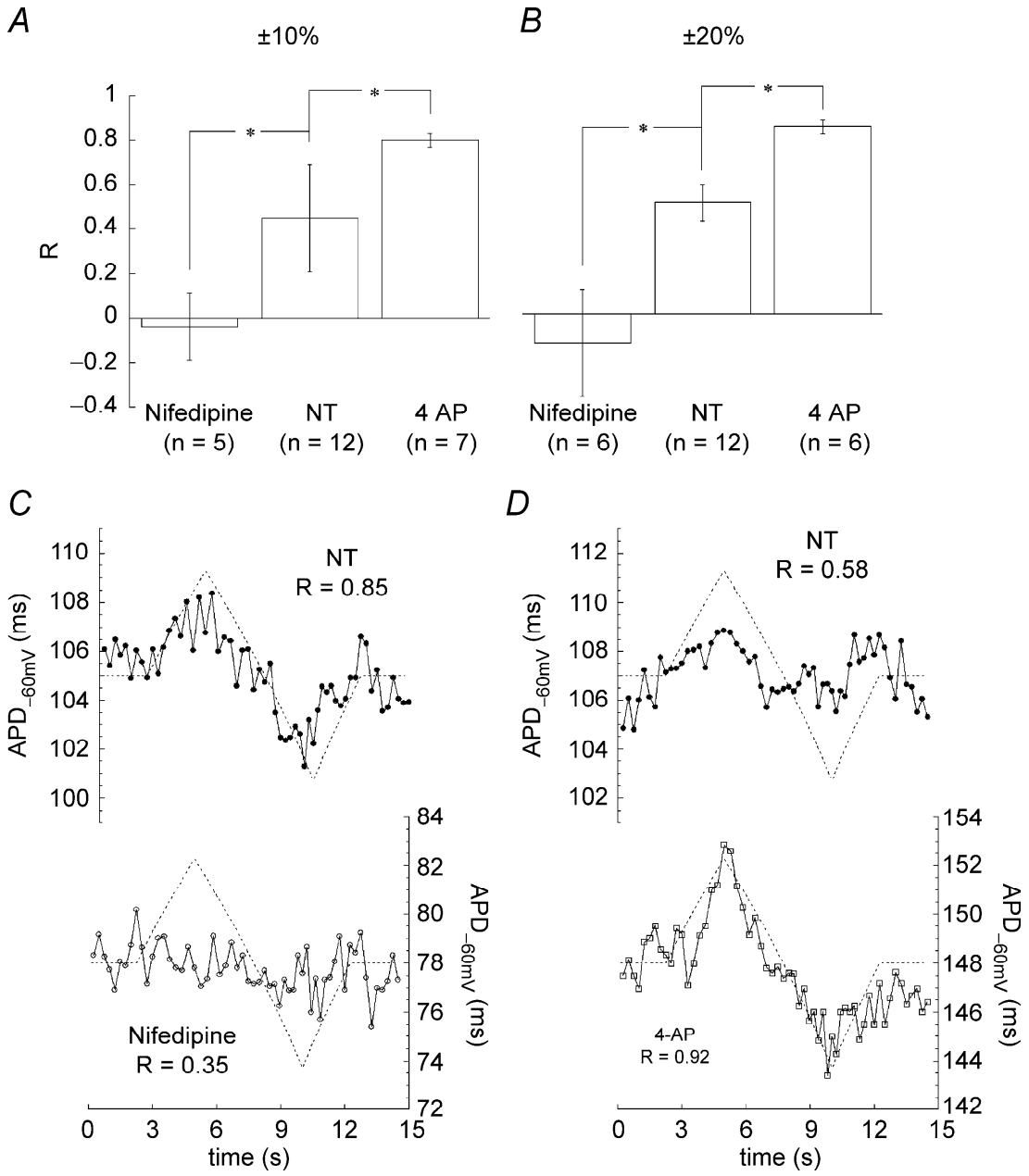

Figure 6. Correlation between $APD_{-60\ mV}$ and linearly changing CL

*A and B, bar graphs representing average value of correlation coefficient (R) between $APD_{-60\ mV}$ and preceding CL during saw-tooth changing pacing rates (see Methods) in ±10 and ±20% CL ranges; effect of blockers (*P < 0.05). C, representative example of $APD_{-60\ mV}$ changes (continuous line, each symbol is 1 beat) for a cell paced with a ±20% saw-tooth changing CL (dotted line), first perfused with NT (upper panel) and then exposed to nifedipine (lower panel). D, same representation for a cell perfused first with NT and then exposed to 4-AP.*

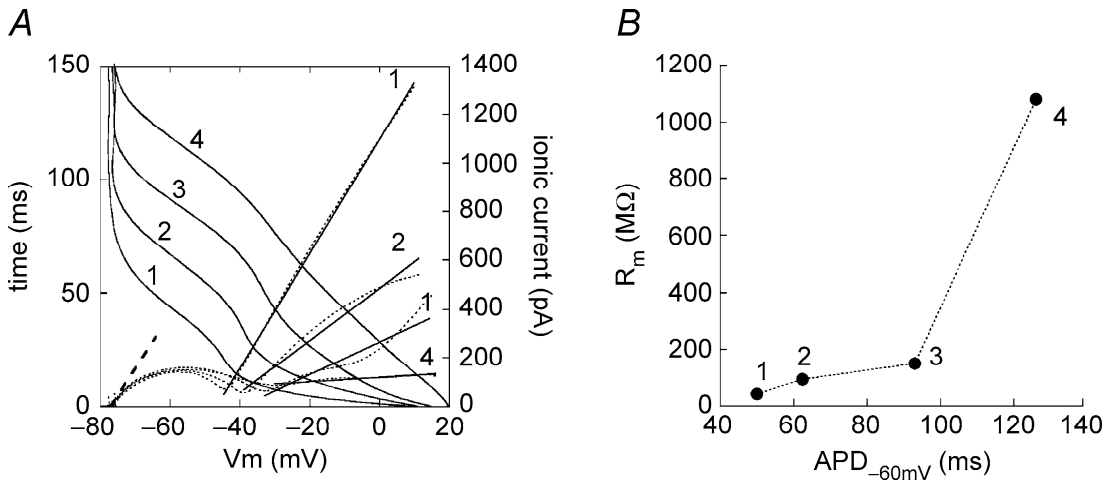

Figure 7. Membrane resistance during early repolarization phase

A, representative repolarization waveforms from 4 different ventricular myocytes paced at 4 Hz (continuous lines, referring to left Y-axis) with superimposed I–V curves (dotted lines, referring to right Y-axis) derived for each AP. Continuous straight lines are linear fittings of I–V curves in the Vm range from the upstroke to the relative minimum value of each I–V function. B, each point corresponds to one AP waveform of A and represents early repolarization Rm value (see Appendix), as a function of the corresponding value of $APD_{-60\ mV}$.

References

Apkon M, Nerbonne J.M. Characterization of two distinct depolarization-activated K^+ currents in isolated adult rat ventricular myocytes. *J Gen Physiol* 97:973-1011,1991.

Bass, B. G. Restitution of the action potential in cat papillary muscle. *Am. J. Phy8i0.* (1975).228, 1717-1724.

Batchvarov V.N, Ghuran A, Smetana P, Hnatkova K, Harries M, Dilaveris P, Camm A.J, Malik M. QT-RR relationship in healthy subjects exhibits substantial intersubject variability and high intrasubject stability. *Am J Physiol Heart Circ Physiol* 282:H2356-H2363,2002.

Carmeliet E. Action potential duration, rate of stimulation, and intracellular sodium. *J Cardiovasc Electrophysiol* (2006). 17, S2–S7.

Clark R.B, Bouchard R.A, Salinas-Stefanon E, Sanchez-Chapula J, Giles W.R. Heterogeneity of action potential waveforms and potassium currents in rat ventricle. *Cardiovasc Res* 27:1795-1799,1993.

Corrado D., Basso C., Thiene G. Sudden cardiac death in young people with apparently normal heart. *Cardiovasc Res* 50:399-408,2001.

Crespo LM, Grantham CJ, and Cannell MB. Kinetics, stoichiometry and role of the Na-Ca exchange mechanism in isolated cardiac myocytes. *Nature* 345: 618–621, 1990.

Earm YE, Ho WK, and So IS. Inward current generated by Na-Ca exchange during the action potential in single atrial cells of the rabbit. *Proc R Soc Lond* 240: 61–81, 1990.

Eisner DA and Lederer WJ. Na-Ca exchange: stoichiometry and electrogenicity. *Am J Physiol Cell Physiol* 248: C189–C202, 1985.

Fabiato A. Simulated calcium current can both cause calcium loading in and trigger calcium release from the sarcoplasmic reticulum of a skinned canine cardiac Purkinje cell. *J Gen Physiol* 85:291–320, 1985.

Fauconnier J, Bedut S, Le Guennec JY, Babuty D & Richard S (2003). Ca2+ current-mediated regulation of action potential by pacing rate in rat ventricular myocytes. *Cardiovasc Res* 57, 670–680.

Fozzard HA. Membrane capacity of the cardiac Purkinje fibre. *J Physiol* 182: 255–267, 1966.

Fozzard H.A, Hanck D.A. Structure and function of voltage-dependent sodium channels: comparison of brain II and cardiac isoforms. *Physiol Rev* 76:887-926,1996.

Fynn SP, Todd DM, Hobbs WJC, Armstrong KL, Fitzpatrick AP & Garratt CJ (2003). Effect of amiodarone on dispersion of atrial refractoriness and cycle length in patients with atrial fibrillation. *J Cardiovasc Electrophysiol* 14, 485–491.

Garfinkel A, Kim YH, Voroshilovsky O, Qu Z, Kil JR, Lee MH, Karagueuzian HS, Weiss JN & Chen PS. Preventing ventricular fibrillation by flattening cardiac restitution. *Proc Natl Acad Sci U S A* (2000). 97, 6061–6066.

Gilmour RF Jr. A novel approach to identifying antiarrhythmic drug targets. (2003). *Drug Discov Today* 8, 162–167.

Gussak I, Wright RS, Bjerregaard P, Chaitman BR, Zhou SH, Hammill SC, Kopecky SL. False-negative and false-positive ECG diagnoses of Q wave myocardial infarction in the presence of right bundle-branch block. *Cardiology.* 2000;94(3):165-72.

Hautala A, Tulppo MP, Makikallio TH, Laukkanen R, Nissila S & Huikuri HV

(2001). Changes in cardiac autonomic regulation after prolonged maximal exercise. *Clin Physiol* 21, 238–245.

Hirao H, Shimizu W, Kurita T, Suyama K, Aihara N, Kamakura S & Shimomura K (1996). Frequency-dependent electrophysiologic properties of ventricular repolarization in patients with congenital Long QT syndrome. *J AmColl Cardiol* 28, 1269–1277.

Janse MJ (2004). Electrophysiological changes in heart failure and their relationship to arrhythmogenesis. *Cardiovasc Res* 61, 208–217.

Janvier NC,McMorn SO, Harrison SM, Taggart P & BoyettMR (1997). The role of Na+–Ca2+ exchange current in electrical restitution in ferret ventricular cells. *J Physiol* 504, 301–314.

Josephson IR, Sanchez-Chapula J and Brown AM. Early outward current in rat ventricular cells. *Circ res.* 1984; 54; 157-162.

Katzung BG, Hondeghem LM, Grant AO. Cardiac ventricular automaticity induced by current of injury. *Pflugers Arch.* 1975;360:193-197.

Koller ML, Riccio ML, Gilmour RF Jr. Dynamic restitution of action potential duration during electrical alternans and ventricular fibrillation. *Am J Physiol.* 1998 Nov;275(5 Pt 2):H1635-42.

Kuo CS, Munakata K, Reddy CP & Surawicz B (1983). Characteristics and possible mechanism of ventricular arrhythmia dependent on the dispersion of action potential durations. *Circulation* 67, 1356–1367.

Laurita KR, Girouard SD, Akar FG, Rosenbaum DS. Modulated dispersion explains changes in arrhythmia vulnerability during premature stimulation of the heart. *Circulation.* 1998 Dec 15;98(24):2774-80.

Lecomte D, Fornes P, Nicolas G. Stressful events as a trigger of sudden death: a

study of 43 medico-legal autopsy cases. *Forensic Sci Int* 79:1-10,1996.

Lee CO, Marban E, Tsien RW. Inactivation of calcium channels in mammalian heart cells: Joint dependence on membrane potential and intracellular calcium. *J Physiol* 364:395-411,1985.

Lesh MD, Pring M & Spear JF (1989). Cellular uncoupling can unmask dispersion of action potential duration in ventricular myocardium. A computer modeling study. *Circ Res* 65, 1426–1440.

Luo CH and Rudy Y. A model of the ventricular cardiac action potential: depolarization, repolarization, and their interaction. *Circ Res* 68: 1501–1526, 1991.

Luo CH and Rudy Y. A dynamic model of the cardiac ventricular action potential. I. Simulations of ionic currents and concentration changes. *Circ Res* 74: 1071–1096, 1994.

Lux R.L., Fuller M.S., Mac Leod R.S., Ersheler P.R., Green L.S., Taccardi B. QT interval dispersion: dispersion of ventricular repolarization or dispersion of QT interval? *J Electrocardiol 30 (suppl)*:176-180,1998.

Maier L.S, Bers D.M, Pieske B. Differences in Ca(2+)-handling and sarcoplasmic reticulum Ca(2+)-content in isolated rat and rabbit myocardium. *J Mol Cell Cardiol* 32(12):2249-58,2000

McMorn SO, Harrison SM & Boyett MR (1998). The effect of temperature on the rate-dependent decrease of the rat ventricular calcium current. *Exp Physiol* 83, 49–63.

Mines GR. On dynamic equilibrium in the heart. *J Physiol* 46: 349–382, 1913.

Myerburg RJ, Interian A, Mitrani RM, Kessler KM, and Castellanos A. Frequency of sudden cardiac death and profiles of risk. *Am J Cardiol* 80: 10F–19F, 1997.

Nanasi PP, Pankucsi C, Banyasz T, Szigligeti P, Papp JG & Varro A. Electrical restitution in rat ventricular muscle. (1996). *Acta Physiol Scand* 158, 143–153.

Pandit SV, Clark RB, Giles WR & Demir SS (2001). A mathematical model of action potential heterogeneity in adult rat left ventricular myocytes. *Biophys J* 81, 3029–3051.

Poggesi C, Everts M, Polla B, Tanzi F & Reggiani C. Influence of thyroid state on mechanical restitution on myocardium. *Circ Res.* 1987. 60, 142-151.

Riccio ML, Koller ML & Gilmour RF Jr (1999). Electrical restitution and spatiotemporal organization during ventricular fibrillation. *Circ Res* 84, 955–963.

Rocchetti M, Malfatto G, Lombardi F & Zaza A (2000). Role of the input/output relation of sinoatrial myocytes in cholinergic modulation of heart rate variability. *J Cardiovasc Electrophysiol* 11, 522–530.

Robinson R.B, Boyden P.A, Hoffman B.F, Hewett K.W. Electrical restitution process in dispersed canine cardiac Purkinje and ventricular cells. *Am J Physiol.* 1987. 253, H1018-H1025.

Rosenbaum DS, Jackson LE, Smith JM, et al. Electrical alternans and vulnerability to ventricular arrhythmias. *N Engl J Med* 330:235-241, 1994.

Sanguinetti M.C., Jurkiewicz N.K. Two components of cardiac delayed rectifier K^+ current. Differential sensitivity to block by class III antiarrhythmic agents. *J Gen Physiol* 96:195-215,1990.

Schipke JD & Pelzer M (2001). Effect of immersion, submersion, and scuba diving on heart rate variability. *Br J Sports Med* 35, 174–180.

Severs NJ, Dupont E, Coppen SR, Halliday D, Inett E, Baylis D & Rothery S (2004). Remodelling of gap junctions and connexin expression in heart disease.

Biochim Biophys Acta 1662, 138–148.

Sgoifo A, De Boer SF, Buwalda B, Korte-Bouws G, Tuma J, Bohus B, Zaagsma J & Koolhaas JM (1998). Vulnerability to arrhythmias during social stress in rats with different sympathovagal balance. *Am J Physiol Heart Circ Physiol* 275, H460–H466.

Shigematsu S, Kiyoshue T, Sato T, Arita M. Rate-dependent prolongation of action potential duration in isolated rat ventricular myocytes. *Basic Res Cardiol* 92:123-128, 1997.

Shipsey S.J., Bryant S.M., Hart G. Effects of hypertrophy on regional action potential characteristics in the rat ventricle. A cellular basis for T-wave inversion? *Circulation* 96:2061-2068,1997.

Sosnowski M, Czyz Z, Tendera M. Scatterplots of RR and RT interval variability bring evidence for diverse non-linear dynamics of heart rate and ventricular repolarization duration in coronary heart disease. *Europace.* 2001 Jan;3(1):39-45.

Surawicz B, Knoebel SB. Long QT: good, bad or indifferent? *J Am Coll Cardiol.* 1984 Aug;4(2):398-413.

Tourner Y, Mitra R, Morad M, Rougier O. Activation properties of the inward-rectifying potassium channel on mammalian heart cells. *J Membr Biol* 97:127-135, 1987.

Watanabe T, Delbridge LM, Bustamante JO & McDonald TF. Heterogeneity of the action potential in isolated rat ventricular myocytes and tissue. (1983). *Circ Res* 52, 280–290.

Watanabe MA & Koller ML. Mathematical analysis of dynamics of cardiac memory and accommodation: theory and experiment. *Am J Physiol Heart Circ Physiol,* (2002). 282, H1534–H1547.

Wilders R, Jongsma H.J. Beating irregularity of single pacemaker cells isolated from the rabbit sinoatrial node. *Biophys J* 65:2601-2613,1993.

Wiswanathan PC, Rudy Y. Pause induced early afterdepolarizations in the long QT syndrome: A simulation study. *Cardiovasc Res* 42:530-542, 1999.

Zabel M,Woosley RL & Franz MR. Is dispersion of ventricular repolarization rate dependent? *Pacing Clin Electrophysiol.* (1997). 20, 2405–2411.

Zaniboni M, Pollard A.E, Yang L, Spitzer K.W. Beat-to-beat repolarization variability in ventricular myocytes and its suppression by electrical coupling. (2000). *Am J Physiol Heart Circ Physiol* 278:H677-H687.

Zaniboni M, Cacciani F & Groppi M. Effect of input resistance voltage-dependency on DC estimate of membrane capacitance in cardiac myocytes. (2005). *Biophys J* 89, 2170–2181.